Rapid CE-UV Evaluation of Polymer-coated Magnetic
Nanoparticles for Selective Binding of Endocrine Disrupting
Compounds and Pharmaceuticals in Water by Aromatic
Interactions

By

Musharraf Miah

A Thesis Submitted to the Faculty of Graduate and Postdoctoral
Affairs in Partial Fulfillment of the Requirements for the Degree of

Master of Science

In

Chemistry Program

Carleton University

Ottawa, Ontario

Library and Archives
Canada

Published Heritage
Branch

395 Wellington Street
Ottawa ON K1A 0N4
Canada

Bibliothèque et
Archives Canada

Direction du
Patrimoine de l'édition

395, rue Wellington
Ottawa ON K1A 0N4
Canada

Canada

Abstract

Endocrine disrupting compounds (EDCs) and pharmaceuticals in water have negative impacts on human health and environmental ecology. Magnetic nanoparticles (MNPs) are currently enjoying a wide range of applications in water treatment. However, these MNPs are not selective to target specific contaminants in complex water matrices. Sorbents that can selectively remove these compounds from drinking water based on their chemical functionality would have a significant health benefit to humans and wildlife. In this work, polydopamine-coated and polypyrrole-coated magnetic nanoparticles (MNPs@PDA and MNPs@PPy) were evaluated as two sorbents for the extraction of bisphenol A (BPA), metformin (MF), naphthalene acetic acid (NAA), phenformin (PF), triclosan (TC) and quinine sulfate (QS). Both in-capillary and *in-vitro* binding efficiencies were determined using capillary electrophoresis with ultraviolet detection (CE-UV). Compared to unmodified MNPs and MNPs@PDA, MNPs@PPy showed higher binding efficiencies. In-capillary binding efficiencies of MNPs@PPy were found to be 99 ± 1% for BPA, PF, TC, and QS. These results were confirmed by *in-vitro* binding tests. Apparently, MNPs@PPy bound strongly with aromatic compounds due to π-π and hydrogen bonding interactions between PPy and analytes. Adsorption isotherms of MNPs@PPy particles revealed higher adsorption capacity (X_m) values for BPA, PF and TC, indicating strong affinity and efficient removal of these target organic compounds from water.

Effective preconcentration is required to produce water samples suitable for instrumental analysis. A mixture of ethyl acetate (EtAc) and methanol (MeOH) (75:25 v/v) was evaluated as a solvent for the elution of preconcentrated compounds and

regeneration of MNPs@PPy particles after each use. Surface regeneration was attempted by putting a new coat of PPy on the used particles. Binding efficiency as high as 94% was achieved for BPA with the regenerated MNPs@PPy particles. Addition of a new coating of PPy proved to be time saving, cost effective and eluent free in recycling the used particles.

Acknowledgements

"All praise belongs to God, the most Merciful, the most Compassionate and the most Gracious"

I would like to express my deepest gratitude to my supervisor, Dr. Edward P.C. Lai for his supervision, advice, and guidance from the early stage of this research as well as for giving me extraordinary experience throughout the work. He provided me encouragement and support in every step.

I gratefully acknowledge Dr. Zafar Iqbal for his kind assistance during this study. It was great pleasure working with him. I am thankful to all colleagues in my group for sharing their experience and knowledge.

I am thankful to Dr. Xun (Daniel) Sun and Mastaneh Azad for their support in the teaching lab. They made my TA job very enjoyable.

I am thankful to Anita Chun (in Prof. P.R. Sundararajan's lab) and Dr. Wendy Hao (in Prof. Wayne Wang's lab) for their technical assistance.

Today, I would like to remember the most valuable person in my life, my mother, who passed away in July, 2011. From my childhood, she always encouraged me in education. Her love and support will never be forgotten. I am thankful to my wife Sonia Afroje Lopa for her patience and inspiration during my M.Sc. study. I also take this opportunity to express my gratitude to my father, brothers, and my sister for their support and encouragement.

Table of Contents

List of Tables

List of Figures

List of Symbols and Abbreviations

[A]	concentration of free adsorbent in the binding equilibrium
B	Longmuir's constant
BGE	background electrolyte
BPA	bisphenol A
CE	capillary electrophoresis
C_e	free adsorbate concentration at equilibrium
C_f	final concentration
DA	dopamine
DDW	deionized distilled water
E	applied electric field
EDCs	endocrine disrupting compounds
EOF	electroosmotic flow
FTIR	fourier transform infrared spectroscopy
fu_{ep}	retarding frictional force
i.d.	internal diameter
K	Freundlich's constant
K	binding constant
k_d	dissociation constant
L_d	effective length of capillary from inlet to detector
L_t	total length of capillary from inlet to outlet
LC-MS/MS	liquid chromatography with tandem mass spectrometry

MF	metformin
MNPs	magnetic nanoparticles
MNPs@PPy	polypyrrole-coated magnetic nanoparticles
MNPs@PDA	polydopamine-coated magnetic nanoparicles
MO	mesityl oxide
M.W	molecular weight
1/n	Freundlich's constant
n	number of binding sites of adsorbent
NAA	naphthalene acetic acid
o.d.	outer diameter
PAHs	polycyclic aromatic hydrocarbons
PDA	polydopamine
PVDF	polyvinylidene fluoride
PF	phenformin
PPCPs	pharmaceutical and personal care products
PPy	polypyrrole
Py	pyrrole
Q	amount of adsorbate bound on the adsorbent particles at equilibrium
QS	quinine sulfate
Q_{max}	apparent maximum binding amount
r	average number of bound adsorbate
SDS	sodium dodecyl sulfate
SEM	scanning electron microscopy

SPE	solid phase extraction
$t_{neutral}$	migration time of neutral marker
TC	triclosan
TGA	thermogravimetric analysis
USEPA	united states environmental protection agency
UV	ultra-violet
u_{ep}	electrophoretic velocity
μ_{eo}	electroosmotic mobility
u_{eo}	electroosmotic velocity
μ_{ep}	electrophoretic mobility
μ_{app}	apparent mobility
XRD	X-ray diffraction
XPS	X-ray photoelectron spectroscopy
X/m	amount of analyte adsorbed by adsorbent
X_m	maximum amount of analyte adsorbed by adsorbent

List of Publications

1. Musharraf Miah, Zafar Iqbal and Edward P.C. Lai, "Rapid CE-UV evaluation of polypyrrole-coated magnetic nanoparticles for selective binding of endocrine disrupting compounds and pharmaceuticals by aromatic interactions", Analytical Methods, 2012, **4**, 2866-2878.

2. Zafar Iqbal, Samar Alsudir, Musharraf Miah and Edward P.C. Lai, "Rapid CE-UV binding tests of environmentally hazardous compounds with polymer-modified magnetic nanoparticles", Electrophoresis, 2011, **32**, 2181-2187.

3. Musharraf Miah, Zafar Iqbal and Edward P.C. Lai, "A comparative CE-UV binding tests study between polypyrrole-coated and polydopamine-coated magnetic nanoparticles with endocrine disrupting compounds and pharmaceuticals in water ", Microchemical Journal, (in progress).

Chapter 1

Introduction

1.1 Contaminants in Drinking Water

Water is a valuable resource and the most significant substance that our bodies require. Without water, human life could not exist on Earth. Only 0.007 percent of all water on the planet is readily accessible for direct human use. According to the government of Ontario, global demand for water will exceed supply by 40 percent by 2030 [1]. When it comes to environmental health, the water industry faces many challenges to ensure a sustained and safe supply of drinking water from sources of varying quality, including the reuse of wastewater [2, 3]. Contaminants that are readily found in environmental and waste water include toxic metals, carcinogenic organic compounds, synthetic chemicals, pharmaceuticals, illicit drugs, cosmetics, personal care products and food supplements, together with their respective metabolites and transformation products [4]. More importance needs to be placed on endocrine disrupting compounds (EDCs), as well as pharmaceutical and personal care products (PPCPs), in order to obtain clean drinking water supplies [5].

Endocrine disrupting compounds (EDCs) are a large group of chemicals that possess the capacity of altering or inhibiting the normal functions of the endocrine system in humans and animals [5]. These compounds can mimic the body's own hormones and may lead to negative health effects. Exposure to EDCs is associated with an early onset of puberty, decreased fecundity/fertility, altered sexual behavior, and abnormalities/cancers of the reproductive tract in humans [6]. The findings of a new study suggest that some endocrine disruptors may play a role in the global epidemic of obesity [7].

Pharmaceuticals and personal care products (PPCPs) illustrate a wide class of chemical contaminants that can originate from human usage/excretions and veterinary applications such as over-the counter, prescription medications and fungicides and disinfectants [8]. According to United States Environmental Protection Agency (USEPA), pharmaceutical compounds are biologically active and certain drugs may cause ecological harm [9]. Although the environmental impact of PPCPs are not fully understood, Environment Canada predicts that long-term exposure to low levels of PPCP residues could have adverse effects on aquatic/terrestrial ecosystems and human health [10]. EDCs and PPCPs are continuously introduced into the aquatic environment from sewage treatment plant effluent, agricultural runoff, concentrated animal feed, landfill leachates, and urban runoff [11, 12]. Direct determination of EDCs in water remains a challenging problem due to their low concentration (fg/L to μg/L). Their detection is further complicated by the presence of numerous other compounds including pharmaceuticals, personal care products, detergents and natural organic matter. Such matrix effects are formidable even when sophisticated instrumental techniques such as liquid chromatography with tandem mass spectrometry (LC-MS/MS) are used [13]. Kibbey *et al.* developed a method for rapid detection of trace EDCs and organic chemicals in natural waters [14, 15]. A UV-transparent polymer-based concentrator served both as a SPE medium to concentrate dissolved chemicals and as an analytical optical cell, allowing rapid quantification of compounds without any labor-intensive pre-concentration procedure. A deconvolution technique was used to determine EDC concentrations in the polymer from UV absorbance spectra. This new preconcentration protocol can potentially be applied to improve the detection limits of EDCs in water analysis.

1.2 Polypyrrole-coated and Polydopamine-coated Magnetic Nanoparticles

Determination of EDCs at ultra-trace levels in environmental water is promising by preconcentration using the molecular adhesive property of polypyrrole (PPy) [16-19]. The structural dimension of solid substrates can influence the partition kinetics, as both submicro- and nano-particles have demonstrated improvements in analyte recovery. Magnetic nanoparticles (MNPs), a kind of nanometer-sized material made of synthetic iron oxides, are widely used in the fields of water treatment [20-23], biotechnology (as an efficient adsorbent with large specific surface area and small diffusion resistance) [24], and nanomedicine (for efficacy of drug delivery and diagnostic imaging) [25].

However, MNPs (such as Fe_3O_4 and Fe_2O_3) can easily form large aggregates, which may alter their magnetic properties. Moreover, these metal oxides are not target-selective in complex sample matrices [26]. Magnetic particles have been coated by different materials such as silica, octadecylsilane, various polymers, and surfactants to preconcentrate pollutants in water [27-34]. Recently, Fe_3O_4 nanoparticles doped with poly (styrene-divinylbenzene-co-4-vinylbenzenesulfonic acid sodium salt) (MPNP) was applied by Zhang et al. for preconcentration of polycyclic aromatic hydrocarbons (PAHs) in environmental water samples via hydrophobic and π-π interaction between MPNP and PAHs [35]. Polypyrrole was applied by Melo et al. as an extraction phase. Its porous structure and multifunctional properties made possible intermolecular interactions like acid-base, π-π, dipole-dipole, hydrogen bonding, and ion exchange between the polymer and analytes [36].

Recently, porous poplypyrrole nanoclusters were applied by Yao et al. for removal of Cr(VI) ions in aqueous solution [37]. The PPy coating also prevents aggregation of the MNPs to improve their dispersibility by enhancing the surface charge for electrostatic repulsion [38]. Upon adding these MNPs@PPy particles into a water sample, the particles will tag a variety of compounds. An external magnetic field is then applied to collect the tagged particles. After desorption of these compounds into a small volume of solvent, spectrofluorimetry, capillary electrophoresis (CE), or LC-MS/MS can be used to perform quantitative analysis. MNPs@PPy particles have been applied by Meng *et al.* to selectively preconcentrate seven phthalates in water samples, for gas chromatography-mass spectrometry analysis, based on π- π interaction between PPy and phthalates [39].

Similarly, dopamine (DA) has been demonstrated to be an effective molecular adhesive that can form a stable polydopamine (PDA) coating on different materials (metals, polymers, and ceramics) [40]. PDA was assembled onto aluminum substrates by simple immersion into DA hydrochloride solution [41, 42]. Recently, Farnard *et al.* used PDA nanoparticles as a new and highly selective biosorbent for the removal of copper (II) ions from aqueous solutions [43]. A self-assembled polydopamine film on the surface of magnetic nanoparticles was used by Zhang *et al.* for specific capture of proteins [44]. MNPs@PDA was applied to bind *Escherichia coli* bacteria from aqueous solution [45]. Figure 1.1 shows the chemical structures of pyrrole, polypyrrole, dopamine and poly dopamine.
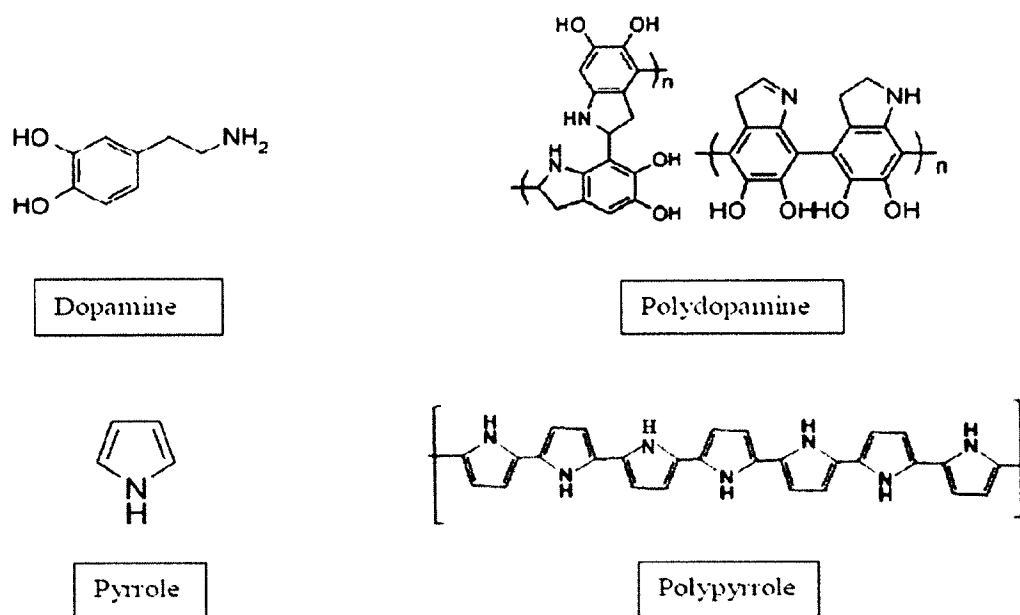
Figure 1.1 Chemical structures of pyrrole, polypyrrole, dopamine and polydopamine.
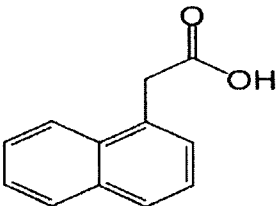
1.3 Capillary Electrophoresis
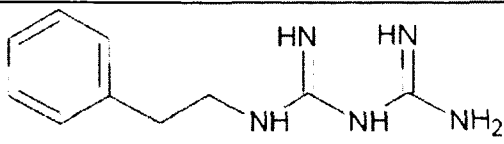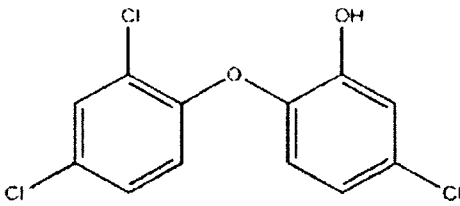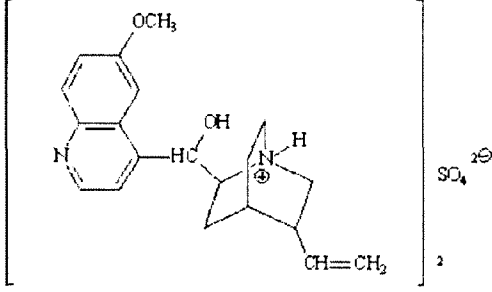
Capillary electrophoresis (CE) is a unique separation technique that, with UV detection, can characterize solid nanoparticles in aqueous suspension [46]. It has been used in analytical separation and characterization of inorganic nanoparticles (Ag, Au, TiO_2, Al_2O_3, Fe_2O_3) [47-51], polystryrene microsphere [52], biomolecules (proteins, peptides) [53, 54], and quantum dots [55]. CE has some advantages over other techniques for characterization of submicron particles, including common availability, short analysis time, clog free operation, high separation efficiency, small volume of buffer and tiny injection of sample [56]. It has undergone intensive development in our laboratory for rapid determination of binding efficiency between environmentally hazardous compounds (bisphenol A, proflavine, naphthalene acetic acid) and

MNPs@PPy and MNPs@PDA [57]. After they were sequentially injected, the compounds and particles overlapped during their migration at different electrophoretic mobilities through the capillary (before they were separated out by CE for UV detection).

In this M.Sc. research, MNPs@PPy and MNPs@PDA particles were evaluated for selective binding with three aromatic EDCs (bisphenol A, naphthalene acetic acid, and triclosan) and three pharmaceutical compounds (metformin, phenformin, and quinine sulfate) in water using CE-UV. The chemical structures and their pK_a values of these target compounds are shown in Table 1.1.

Table 1.1 Chemical structures and pK_a values of target compounds.

Analyte (Abbreviation)	Chemical Structure	pK_a
Bisphenol A (BPA)		9.6 [58]
Metformin (MF)		12.4 [59]
Naphthalene acetic acid (NAA)		4.2 [57]

Phenformin (PF)		11.3 [60]
Triclosan (TC)		8.1 [61]
Quinine sulfate (QS)		8.5 [62]

1.4 Research Goals

The aims of this research were to synthesize MNPs, MNPs@PDA, MNPs@PPy particles and evaluate these magnetic nanoparticles (unmodified and polymer-coated) for selective binding with EDCs and PPCPs in water by CE-UV. Their binding efficiency with BPA, NAA, MF, PF, TC, and QS was investigated. These particles were characterized by fourier transform infrared spectroscopy (FTIR), scanning electron microscopy (SEM), thermogravimetric analysis (TGA), and X-ray diffraction analysis (XRD). The adsorption kinetics and adsorption isotherms of these target compounds were also studied.

The ultimate goal of this research was to use these particles as magnetic sorbents for the preconcentration of target compounds in future water analysis.

Chapter 2

Principle of

Capillary Electrophoresis

and

Theory of

Adsorption Isotherms

2.1 Principle of Capillary Electrophoresis

Electrophoresis is a process for separating charged molecules or ions based on the migration of the molecules through a solution under the influence of an applied electric field. As illustrated in Figure 2.1, the positively charged molecules or ions are attracted to the negative electrode (cathode) and negatively charged molecules or ions are attracted to the positive electrode (anode). A carrier electrolyte (also known as background electrolyte or run buffer) is required to maintain the necessary pH and to provide sufficient conductivity. This allows the passage of current necessary for the separation [63].
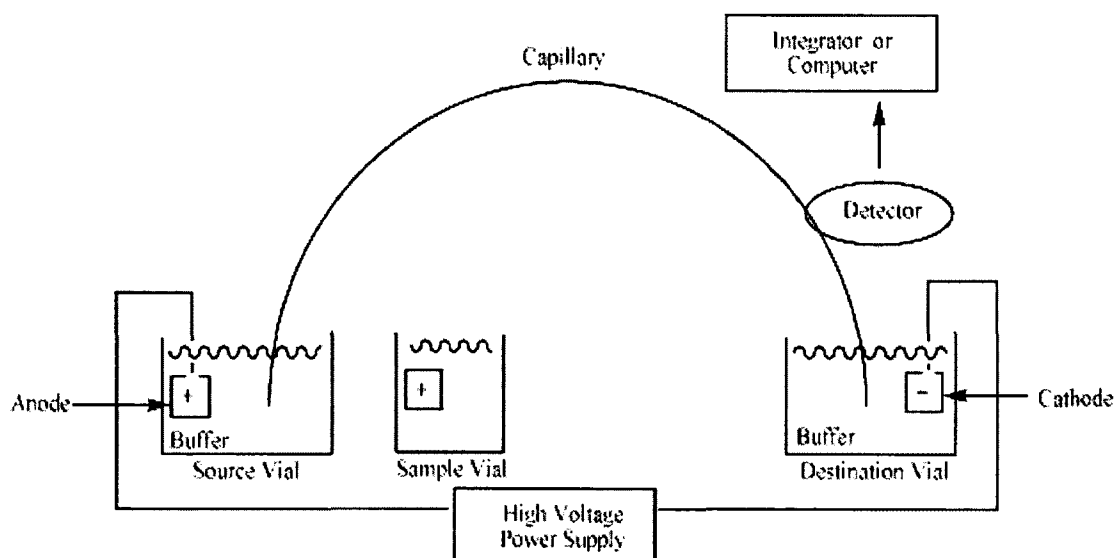
Figure 2.1 Typical instrumental set up of capillary electrophoresis [64].

2.1.1 Electrophoretic mobility

When an electric field E (V/m) is applied on a charged ion or species (q), the force on the species is equal to qE (newtons). The movement of the ion or species is also influenced by the retarding frictional force fu_{ep}. When the frictional force equals the accelerating force, the ion rapidly reaches a constant velocity $(fu_{ep} = qE)$.

Electrophoretic velocity: $u_{ep} = (q/f) E = \mu_{ep} E$ $\qquad$ (2-1)

where μ_{ep} is the electrophoretic mobility, which is the constant of proportionality between the ion velocity and the electric field strength.

2.1.2 Electroosmotic flow

Electroosmotic flow (EOF) illustrates the movement of ions through a solute under the control of an applied potential. The inner wall of a fused silica capillary is covered with silanol groups (Si-OH) and at pH higher than 2 are negatively charged (Si-O⁻). The fixed negative charge on the inner wall and the excess cations near the wall result in a double layer. The tightly adsorbed layer of the cations neutralizes partially the negative charges on the capillary wall and the remaining negative charges of the capillary are neutralized by mobile cations that are in diffuse part of the double layer in the solution near the wall.

In an electric field, cations are migrated towards the cathode while anions are pulled towards the anode. A net momentum towards the cathode is produced by the excess cations in the diffuse part of the double layer. These cations drive a pumping action

called electroosmosis and eventually create a uniform electroosmotic flow (EOF) of the entire solution towards the cathode as shown in the Figure 2.2 [65].
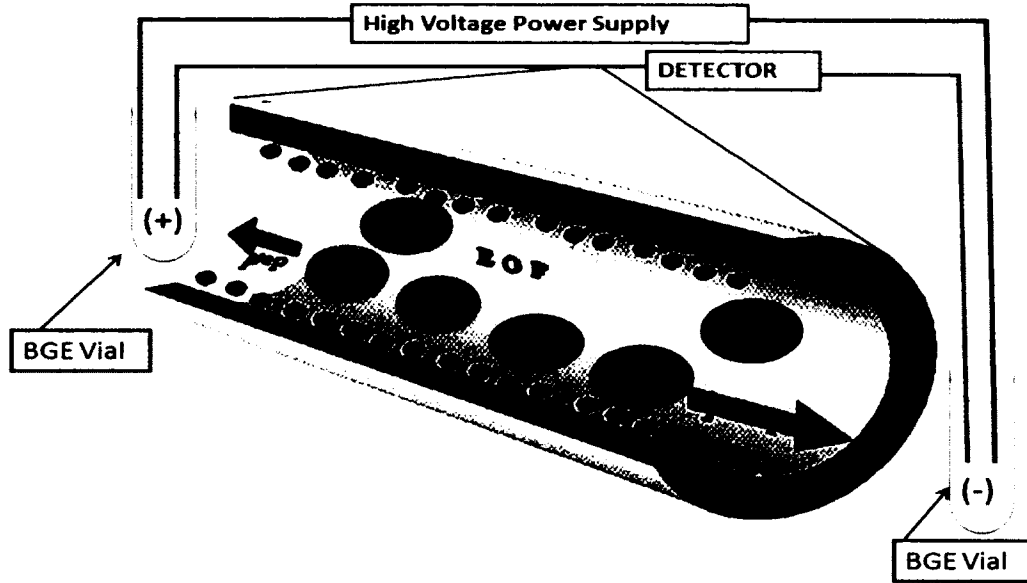
Figure 2.2 Electroosmotic flow (EOF) towards the cathode driven by the cations in the diffuse part of the double layer.

Electroosmotic flow is the constant of proportionality between the electroosmotic velocity (u_{eo}) and the strength of the applied electric field (E).

$$u_{eo} = \mu_{eo}\, E \tag{2-2}$$

where μ_{eo} is the electroosmotic mobility

$$u_{eo} = (L_d / t_{neutral}) \tag{2-3}$$

where L_d is the effective length of the capillary (to the detector) and $t_{neutral}$ is the migration time of a neutral marker.

Electroosmotic mobility $\mu_{eo} = u_{eo} / E = (L_d / t_{neutral}) / (V / L_t)$ (2-4)
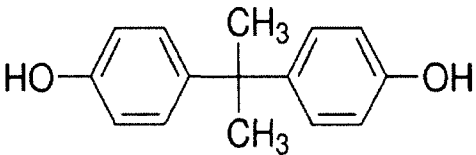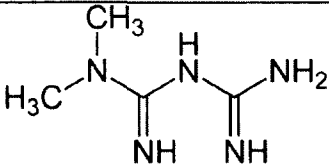
where L_t is the total length of the capillary.

Uniform EOF provides high resolution of capillary electrophoresis and if disturbed, can cause peak broadening. The flow of ions in the capillary produces joule heating which causes the solution viscosity to decrease, therefore disturbing the flat profile of the EOF. Hence, the capillary inner diameter should be adequately small, ranging from 20 to 200 μm to rapidly dissipate the generated heat [66].

2.1.3 Apparent Mobility

Mobility or apparent mobility, μ_{app}, of an ion can be defined as the sum of the electrophoretic mobility of the ion and the electroosmotic mobility of the solution.

Apparent mobility $\mu_{app} = \mu_{ep} + \mu_{eo}$ (2-5)

Cations migrate along with the EOF direction. Therefore, μ_{ep} and μ_{eo} have the same sign, resulting a greater value to μ_{app} than μ_{ep} ($\mu_{app} = \mu_{eo} + \mu_{ep}$). On the other hand, anions migrate in the opposite direction of the EOF. Thus μ_{ep} and μ_{eo} have opposite signs, resulting a lesser value to μ_{app} than μ_{ep} ($\mu_{app} = \mu_{eo} - \mu_{ep}$). The apparent mobility of a neutral analyte equals the electroosmotic mobility of the solution ($\mu_{app} = \mu_{eo}$). Figure 2.3 shows the Electroosmotic flow and apparent electrophoretic mobility using normal polarity configuration.
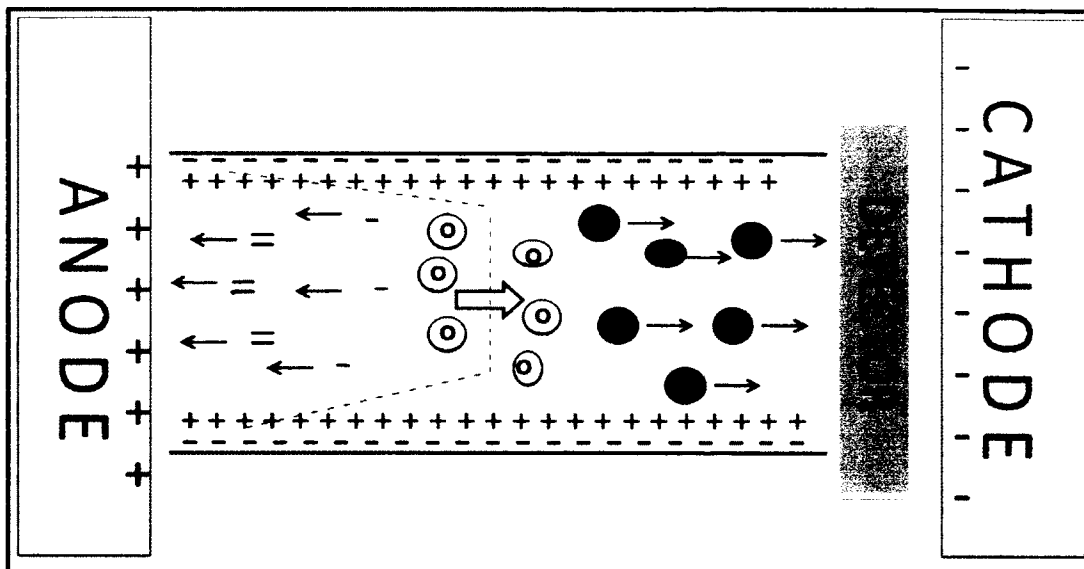
Figure 2.3 Electroosmotic flow and apparent electrophoretic mobility using normal polarity configuration.

The apparent mobility of an ion or species is the net velocity of the ion, u_{net}, divided by the electric field, E.

$$\mu_{app} = u_{net} / E = (Ld / t) / (V / Lt) \tag{2-6}$$

where t is the migration time of the ion or species.

The electrophoretic mobility, μ_{ep}, is the difference between apparent mobility and electroosmotic mobility ($\mu_{ep} = \mu_{app} - \mu_{eo}$). The electrophoretic mobility of an analyte should not be affected by discrepancies from run to run since it is measured in relation to a neutral analyte [67].

14

2.2 Theory of Adsorption Isotherms

Adsorption isotherm can be defined as a graphical representation of the relationship between the activity of adsorbate and adsorbent at constant temperature. Equilibrium adsorption isotherm illustrates the interaction between the adsorbate and the adsorbent. An insight into both the sorption mechanism and affinity of the adsorbent can be explained by determining the adsorption capacity of an adsorbent and modeling of isotherms by different equilibrium models [68]. There are different isotherm models have been applied by many researchers to explain binding chemistry. The commonly used models are Freundlich, Langmuir, Klotz and Scatchard isotherm models. Each isotherm is a unique model of the binding events.

In 1909, Freundlich expressed an empirical equation for representing the isotherm variation of adsorption of a quantity of adsorbate adsorbed by unit mass of solid adsorbent with pressure. Freundlich equation can be shown as:

$$X/m = K\, C_f^{1/n} \qquad (2\text{-}7)$$

The linear form of the equation is:

$$log X/m = log K + 1/n\, log C_f \qquad (2\text{-}8)$$

where K (mg.g^{-1}) and $1/n$ are Freundlich's constants indicating adsorption capacity and intensity of adsorption, respectively [69]. Mostly, logX/m versus logC_f is plotted for a Freundich adsorption isotherm. The value of K indicates the affinity of adsorbent to adsorbate.

The Langmuir adsorption equation was developed by Irving Langmuir in 1916 for gases adsorbed on solids. Later on, this model was used by many researchers for other compounds adsorbed by various adsorbent materials. Langmuir equation can be shown as:

$$X/m = X_m \, b \, C_f / 1 + b \, C_f \qquad (2\text{-}9)$$

The linear form of the equation is:

$$m/X = X_m + 1/X_m \, b \, C_f \qquad (2\text{-}10)$$

where X/m is the amount of analyte or adsorbate adsorbed by adsorbent ($\mu mol.g^{-1}$), X_m is the maximum amount of analyte adsorbed ($\mu mol.g^{-1}$), C_f is the final concentration of analyte ($\mu mol.L^{-1}$) at equilibrium, and b ($L.\mu mol^{-1}$) is a Langmuir constant signifying the energy of sorption [69]. Generally, m/X versus $1/C_f$ is plotted for Langmuir isotherm and the values of X_m and b are calculated from the linear equation of Langmuir's adsorption isotherm. ($X_m = 1/$ intercept, and b $= 1/$slope$.X_m$). The value of X_m determines the binding capacity of the adsorbent.

Klotz equation provides the relationship between the average numbers of bound adsorbate (r) and the concentration of free adsorbate ([A]) in the binding equilibrium.

The Klotz equation can be illustrated as:

$$r = (1/nk) \, (1/[A]) + 1/n \qquad (2\text{-}11)$$

where n is the number of binding sites of adsorbent and k is the binding constant. Generally, 1/r against 1/ [A] is plotted and n and k are calculated from a regressing equation [70].

The Scatchard plot is used for the evaluation of adsorption parameters. This plot can indicate how many kind of binding sites exist in the adsorbent particles.

The Scatchard equation can be written as:

$$Q/C_e = (Q_{max} - Q)/K_d \qquad (2\text{-}12)$$

where Q is the amount of adsorbate bound on the adsorbent particles at equilibrium; C_e is the free adsorbate concentration at equilibrium; K_d is the dissociation constant and Q_{max} is the apparent maximum binding amount. The values of K_d and the Q_{max} can be calculated from the slope and the intercept of the linear line plotted in Q/C_e versus Q [71].

Chapter 3

Experimental

3. Experimental

3.1 Materials

Acetic acid (CH_3COOH), ammonium hydroxide (NH_4OH), bisphenol A (BPA), iron(II) chloride tetrahydrate ($FeCl_2.4H_2O$), iron(III) chloride hexahydrate ($FeCl_3.6H_2O$), mesityl oxide (MO), metformin hydrochloride (MF.HCl), naphthalene acetic acid (NAA), phenformin (PF), pyrrole (Py), dopamine hydrochloride (DA.HCl), disodium hydrogen phosphate (Na_2HPO_4), sodium dodecyl sulphate (SDS), potassium bromide (KBr), triclosan (TC), and quinine sulfate (QS) were obtained from Sigma-Aldrich (Oakville, ON, Canada). HPLC-grade methanol (MeOH) and ethyl acetate (EtAc) were purchased from Caledon (Georgetown, Ontario, Canada). All chemicals were used as received without any further purification.

3.2 Apparatus and Analytical Method

CE-UV analysis was performed on a laboratory-built system including a Spellman CZE1000R high voltage power supply (Hauppauge, New York, USA). Fused-silica capillary (51 μm i.d., 356 μm o.d. and 16 μm polyimide coating) was obtained from Polymicro Technologies (Phoenix, AZ, USA). The background electrolyte (BGE) was composed of 20 mM Na_2HPO_4 in deionized distilled water (DDW) to attain pH 8.5 ± 0.2. Prior to initial use of a capillary, a typical conditioning procedure was followed. The capillary was reconditioned by flushing with methanol (MeOH), 1.0 M HCl, 1.0 M NaOH, deionized distilled water (DDW) and BGE for 15 min. After extended use of the capillary, it was reconditioned quickly by flushing the capillary with MeOH, 1.0 M HCl,

1.0 M NaOH, DDW, and BGE for 3 min each. The capillary was finally equilibrated with the BGE at an applied voltage of 20 kV for 10 min. A Bischoff Lambda 1010 (Leonberg, Germany) UV detector was employed, at a wavelength of 200 nm, to detect the migration of analytes. This 200 nm of wavelength was selected based upon the absorption spectrum of BPA. The detector output signal was acquired through a Peak Simple Chromatography Data System (SRI model 203, Torrance, CA, USA). The BGE was run at 20 kV for 1 min in between sample analyses to eliminate the possibility of carryover. The capillary inlet and outlet BGEs were changed after every ten CE analyses to maintain its purity and level in the vials. The capillary inlet was kept 2 mm away (d) and below (h) the electrode as shown in Figure 3.1 to improve both precision and baseline stability.
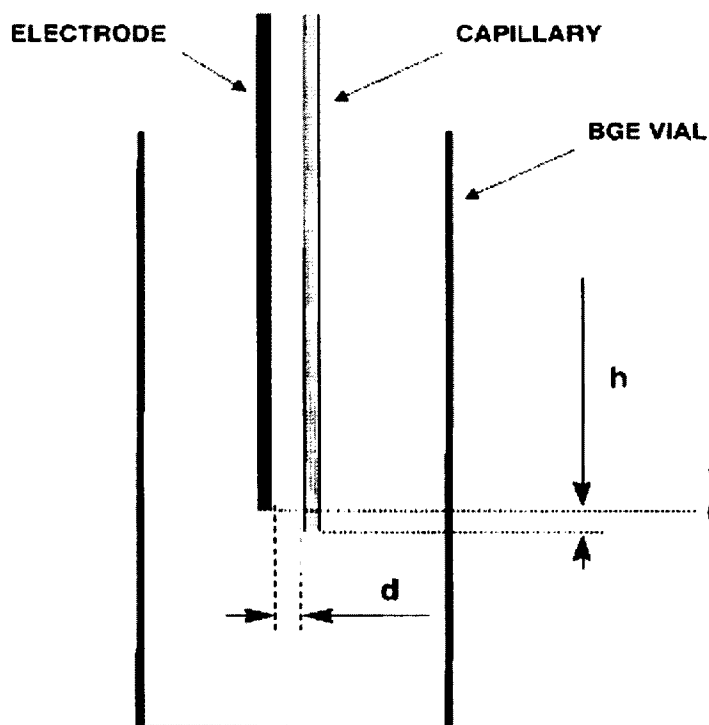
Figure 3.1 Relative positions of the capillary inlet and electrode in background electrolyte (BGE) vial [72].

3.3 Preparation of Polypyrrole-coated and Polydopamine-coated Magnetic Nanoparticles

MNPs (Fe_3O_4) were prepared using a method previously described by Wang *et al.* [73]. First, MNPs were synthesized through co-precipitation of Fe^{2+} and Fe^{3+} ions in solution, in the presence of excess NH_4OH, under nitrogen gas flow. 160 mL DDW was deaerated under nitrogen for 30 min. 3.44 g $FeCl_2.4H_2O$ and 9.44 g $FeCl_3$ was dissolved in 160 mL of deaerated DDW contained in a three neck flask equipped with a mechanical stirrer. The mixture was vigorously stirred to get a homogenous mixture. As the temperature reaches 78-80 °C, 20 mL of ammonium hydroxide was introduced to the three neck flask drop by drop, and the reaction was continued for 30 min. The black Fe_3O_4 (MNPs) was separated by using a magnet and the supernatant was decanted. The black MNPs were washed five times with DDW to remove unreacted chemicals. The MNPs then air dried in the fume hood for 48 hours.

They were next coated with PPy using a procedure reported by Meng *et al.* [39], with some modifications as shown in Figure 3.2(b). 400 mL of DDW was deaerated by bubbling nitrogen for 30 min in a 500-mL three-necked round-bottomed flask equipped with a mechanical stirrer as shown in Figure 3.2(a). Then 0.44 g of SDS was added and the solution was stirred for 10 min. Next 0.20 g of MNPs was added to the flask and the suspension was stirred for 30 min. Finally 2.0 mL of pyrrole was added and the suspension was stirred for 1 hour to achieve a complete dispersion. Polymerization was performed, using $FeCl_3.6H_2O$ as an oxidant at 22(±1) °C for 12 hours with gentle stirring. Hence 1.1 g of this oxidant, dissolved in 20 mL of DDW, was added drop by drop to allow homogeneous mixing with the suspension. Finally the black MNPs@PPy particles

21

was separated by a magnet, washed with DDW and MeOH (5 times each), and air-dried in the fume hood for 48 hours.

(a)

(b)
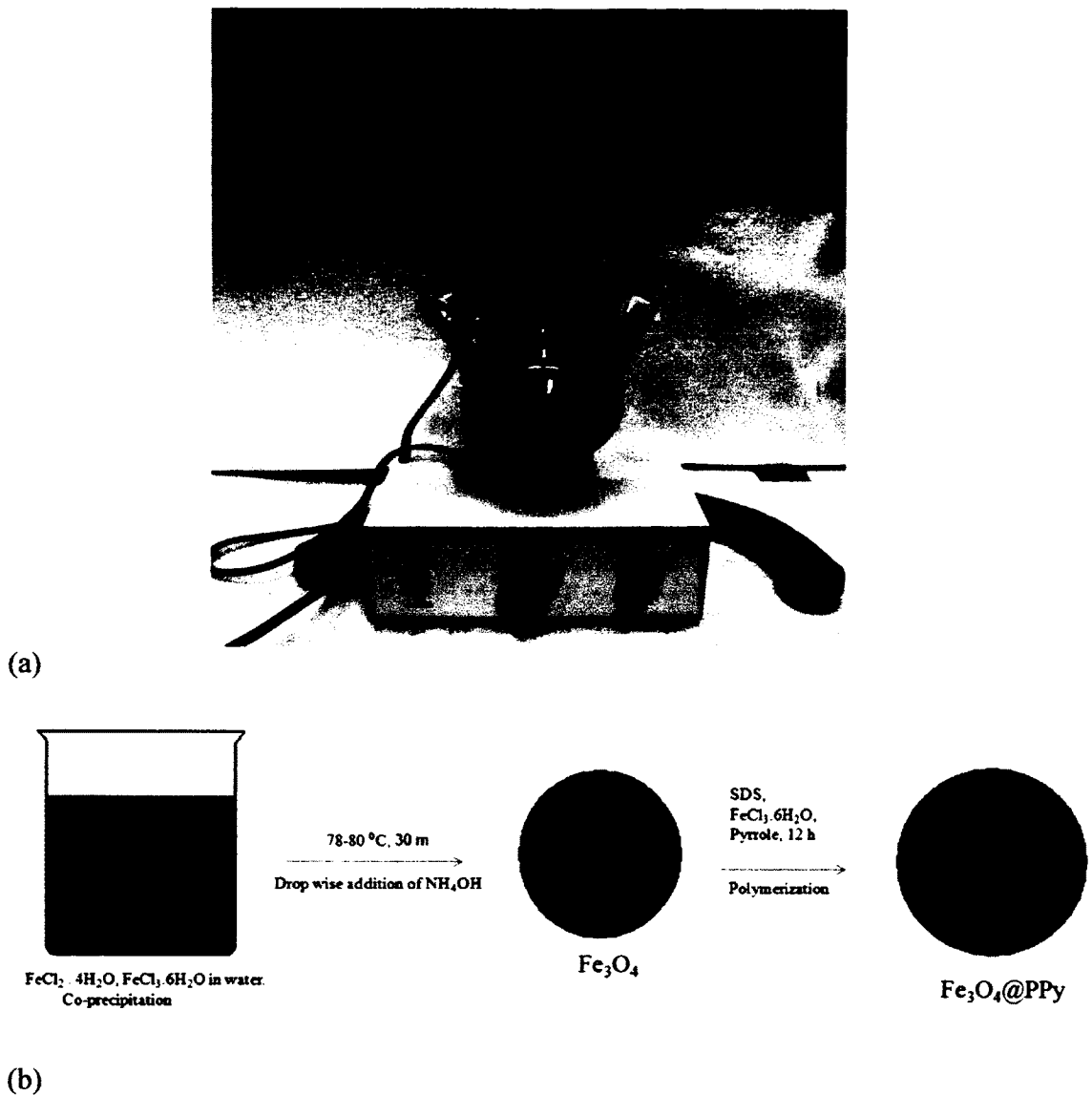
Figure 3.2(a) Experimental setup for coating MNPs with PPy or PDA, (b) Schematic illustration of Fe_3O_4 and Fe_3O_4@PPy syntheses.

Coating of MNPs with PDA was adopted from the method reported by Yang and co-workers with some modifications [74]. 2.63 g of MNPs were added into 500 mL of 10 mM Na_2HPO_4 (pH 7.5 ± 0.2) buffer in a 500-mL three-necked round-bottomed flask equipped with a mechanical stirrer. The mixture was stirred for 2 hours until the nanoparticles were well-dispersed. Then 1.0 g of DA was added and the reaction mixture was stirred for another 3 hours at room temperature. The product was collected with a magnet and washed five times with 3% (v/v) acetic acid containing 0.1% (w/w) SDS, and then with DDW. The black MNPs@PDA particles were air-dried in the fume hood for 48 hours.

3.4 In-capillary binding test

Samples containing MNPs, MNPs@PPy and MNPs@PDA particles (10 mg.mL^{-1}), analytes (BPA, MF, NAA, PF, and QS, 200 µg.mL^{-1}) and neutral marker (MO) (0.1% v/v) were prepared in 20 mM BGE for CE-UV analysis. Triclosan (200 µg.mL^{-1}) was prepared in MeOH/BGE (20:80 v/v). The capillary was first reconditioned as described in section 3.2. Electrokinetic injections (1st injection of MNPs or MNPs@PPy or MNPs@PDA particles for 48 s, and 2nd injection of analytes for 3 s) at 17 kV were performed for CE-UV analysis or binding test. A standard calibration curve was constructed by performing triplicate CE analyses of each analyte concentration. After each binding test (of analytes with MNPs or MNPs@PPy or MNPs@PDA particles), the capillary was quickly washed with MeOH, 1.0 M HCl and BGE for 2-3 min each. All

binding tests were carried out in triplicates, and the % binding of the analytes was calculated as followed:

% binding = [(peak area of analyte before binding – peak area of analyte after binding) / peak area of analyte before binding] x 100   (3-1)

3.5 *In-vitro* binding and desorption tests

A two-step procedure was followed to carry out *in-vitro* binding tests in water samples and desorption tests with an appropriate eluent. Stocks of analyte solutions (MF, PF and NAA, 2000 $\mu g.mL^{-1}$) were prepared separately in 20 mM BGE. BPA (500 $\mu g.mL^{-1}$) and QS (1000 $\mu g.mL^{-1}$) were also prepared separately in 20 mM BGE. Triclosan (TC) solution (2000 $\mu g.mL^{-1}$) was prepared in MeOH/BGE (20:80 v/v). 4 mL each of four analyte solutions (MF, PF, NAA, and TC), 8 mL of QS and 16 mL of BPA solutions were thoroughly mixed (total volume of 40 mL) in a single container in order to achieve 200 $\mu g.mL^{-1}$ of each analyte. 2 mL of the mixture solution containing six analytes (BPA, MF, PF, NAA, TC, and QS, 200 $\mu g.mL^{-1}$) was poured into a 2 mL vial. Next 18 mg of MNPs or MNPs@PDA or MNPs@PPy particles were added. The vial containing the particles and six analytes was sonicated for 2 min and shaken using a Bioshaker (1500 rpm and at 25°C) for 10 min. Then a magnet was placed under the vial for 10 min to bring down the MNPs or MNPs@PPy or MNPs@PDA particles, and 2 mL of the supernatant was poured into a clean vial for CE-UV analysis (in the 1st injection for 3 s at 17 kV) to determine any remaining analytes. For desorption of the bound analytes on MNPs@PPy particles, a 3:1 (v/v) mixture of ethyl acetate (1.5 mL) and MeOH (0.5 mL)

were added to the vial. After 10 min of sonication, the MNPs@PPy particles were brought down by a magnet over 10 min. 2 mL of supernatant containing the desorbed analytes were poured out for CE-UV analysis to determine any desorbed analytes. 2 mL of mixture solution containing the six analytes (200 $\mu g.mL^{-1}$ each) were also analyzed by CE-UV to compare the peak areas with those obtained above for the supernatant. The % non-binding of the analytes was calculated as followed:

% Non-binding = (Peak area of analyte in supernatant / Peak area of analyte in mixture solution) x 100   (3-2)

3.6 Adsorption kinetics and adsorption isotherms

Adsorption kinetics was studied by calculating the time of each analyte overlapping with MNPs@PPy during the CE-UV binding test. This time of overlap was equal to the half width of MNPs@PPy peak divided by the difference in migration velocity between the analyte and MNPs@PPy peaks. The half width of MNPs@PPy peak (in millimeters) was calculated as the width of MNPs@PPy peak at half of the maximum height (in seconds) x migration velocity of MNPs@PPy (in millimeters/second). The migration velocity of analyte was given by the length of capillary from inlet to detection window (in millimeters) divided by the migration time of analyte (in seconds). Similarly, the migration velocity of MNPs@PPy was given by the length of capillary from inlet to detection window divided by the migration time of MNPs@PPy.

Adsorption isotherms were studied in a batch mode by dissolving each analyte in 20 mM BGE (pH 8.5 ± 0.2) at a known concentration (from 100 to 1000 $\mu g.mL^{-1}$) in a 2-mL vial.

After 18 mg of MNPs@PPy were added, the mixture was shaken at 1500 rpm for 20 min at room temperature (25 °C). The mixture was then centrifuged for 5 min, and the supernatant was collected in a 2-mL glass vial for analysis by CE-UV. The peak areas from standard analyte solutions and the collected supernatant were compared to calculate the % binding (%B). The amount of analyte adsorbed onto a unit mass of the adsorbent, X/m ($\mu mol.g^{-1}$), at equilibrium was calculated using

$$X/m = (\%B \times C_o \times V) / (100 \ m) \hspace{3cm} (3\text{-}3)$$

In this equation, C_o is the initial concentration of analyte ($\mu mol.L^{-1}$), m is the weight of MNPs@PPy (g), and V is the volume of analyte solution (L).

3.7 Characterization of MNPs@PPy and MNPs@PDA particles by SEM and FTIR

Dry MNPs, MNPs@PPy and MNPs@PDA particles were placed onto individual carbon tapes and coated with 6 nm of gold using an RF sputtering system (Anatech Hummer VII, Union City, CA, USA). The particles were analyzed by scanning electron microscopy (SEM) (Tescan Vega II, XMU, Cranberry, PA, USA) at an accelerating voltage of 15 kV. For analysis by Fourier transform infrared spectroscopy (FTIR) (ABB Bomem MB Series, Quebec, Canada), MNPs, MNPs@PPy and MNPs@PDA particles (~2 mg) were ground with dehydrated KBr in separate mortars with a pestle. These mixtures were pressed in a mould to form discs for FTIR analysis immediately.

3.8 Thermogravimetric and X-ray-diffraction analysis of MNPs and MNPs@PPy

Thermogravimetric analysis (TGA) of MNPs, MNPs@PPy and PPy were performed on ~8 mg of sample using a Hi-Res TGA 2950 Thermogravimetric Analyzer (TA Instruments, New Castle, DE, USA). The heating rate was 10 °C min^{-1}, and the nitrogen flow rate was 50 mL.min^{-1}.

X-ray diffraction data were collected within the range of 3°≤2θ ≤70° for both MNPs and MNPs@PPy particles using a Philips PW 1710 automated powder diffractometer attached to a 2000-watt nickel-filtered Cu K$_\alpha$ radiation source (λ = 1.542Å). The data was collected by MDI Data Scan 3.2 software (Materials Data, Livermore, CA, USA) and the results were analyzed using MDI Jade 5.0 XRD Pattern Processing software.

3.9 Regeneration of MNPs@PPy particles

BPA was prepared (200 μg.mL^{-1}) in a vial containing 2 mL of 20 mM BGE. Next 18 mg of MNPs@PPy particles was added. The vial was sonicated for 2 min and shaken using the bioshaker (1500 rpm) at 25 °C for 10 min. Then a magnet was placed under the vial for 10 min to bring down the MNPs@PPy particles, and the supernatant was poured into a 2-mL vial for CE-UV analysis to determine any remaining BPA. The BPA-bound MNPs@PPy particles were coated again by repeating the same procedure as described in Section 3.3. Finally the black regenerated MNPs@PPy particles was separated by a magnet, washed with DDW and MeOH (5 times each), and air-dried in fume hood for 48 hours.

3.10 Application to river water analysis

A river water sample was collected in a glass bottle from the Rideau River in Ottawa. A 0.22 μm polyvinylidene fluoride (PVDF) filter was used to remove soil particles contained in the river water. Background electrolyte (BGE) was prepared by adding 0.14 g of Na_2HPO_4 in 50 mL of filtered river water (20 mM, pH 8.5 ± 0.2). 2.0 mg of PF was spiked into 10 mL of filtered river water to prepare 200 $\mu g.mL^{-1}$ PF. The filtered and spiked river water samples were tested by CE-UV. For binding test with MNPs@PPy, the spiked river water sample was 2nd injected for 3 s and MNPs@PPy particles was 1st injected for 48 s, both at 17 kV.

Chapter 4

Results and Discussion

4.1 Coating of MNPs with PPy and PDA

Figure 3.2(b) shows the two-step procedure to synthesize MNPs@PPy particles. The synthesis of MNPs was simple. The coating of MNPs with PPy was slightly modified from the procedure reported by Meng *et al.* [39]. Surfactant is usually needed for stabilizing the dispersion of MNPs during coating with PPy. Instead of sodium dodecyl benzene sulfonate (NaDBS), SDS was used as an inexpensive anionic surfactant that is commercially available. Also, the PPy concentration was decreased by half in order to achieve a reasonable coating thickness. In the synthesis of MNPs@PDA, disodium hydrogen phosphate buffer was used instead of tris buffer, since the same buffer was used as BGE for subsequent CE-UV analysis. In comparison to the MNPs@PPy procedure, the preparation of MNPs@PDA was fast and simple. The polymerization of dopamine took only 3 hours compared to 12 hours for pyrrole. Also, no oxidizing agent was required for dopamine polymerization [75].

4.2 FTIR spectra of MNPs, MNPs@PPy and MNPs@PDA

The MNPs, MNPs@PPy and MNPs@PDA particles were characterized by FTIR, as shown in Figure 4.1(a) (b). Three characteristic peaks at 3452, 1632, and 592 cm^{-1} were observed for Fe_3O_4 nanoparticles. The absorption band at 592 cm^{-1} corresponds to Fe-O bond of bulk magnetite (lit., [76] 585 cm^{-1}, [77] 620 cm^{-1}). Some additional bands appear from 1555 to 621 cm^{-1} after coating MNPs with PPy. The characteristic peaks of PPy at 1555 cm^{-1} and 1468 cm^{-1} correspond to the anti-symmetric and symmetric C=C stretching vibrations of the Py rings, respectively (lit., [39] 1538 cm^{-1} and 1450 cm^{-1}, [60]

1556 cm^{-1} and 1460 cm^{-1}, [78] 1548 cm^{-1} and 1466 cm^{-1}). The bands at 1316 cm^{-1} and

1044 cm^{-1}, can be attributed to the C-N stretching vibrations and C-H deformation

vibrations (lit., [60]1315 cm^{-1} and 1043 cm^{-1}, [78] 1300 cm^{-1} and 1050 cm^{-1}). Bands at

1190 cm^{-1}, 917 cm^{-1} and 790 cm^{-1} are related to =C-H in-plane and out-of-plane

vibrations of Py, as previously reported (lit., [39] 1162 cm^{-1}, 887 cm^{-1}, 775 cm^{-1}). The

characteristic peak of MNPs at 592 cm^{-1} is absent in the MNPs@PPy spectrum partly due

to the thick PPy coating that suppressed the MNPs peak. Also, the appearance of two

dominant peaks at 917 cm^{-1} and 1190 cm^{-1} indicates that the MNPs@PPy spectrum

cannot be simply taken to be the sum of the MNPs and PPy spectra. Chemical

interactions between the MNPs and PPy have likely occurred to alter the vibrational

modes in MNPs@PPy.
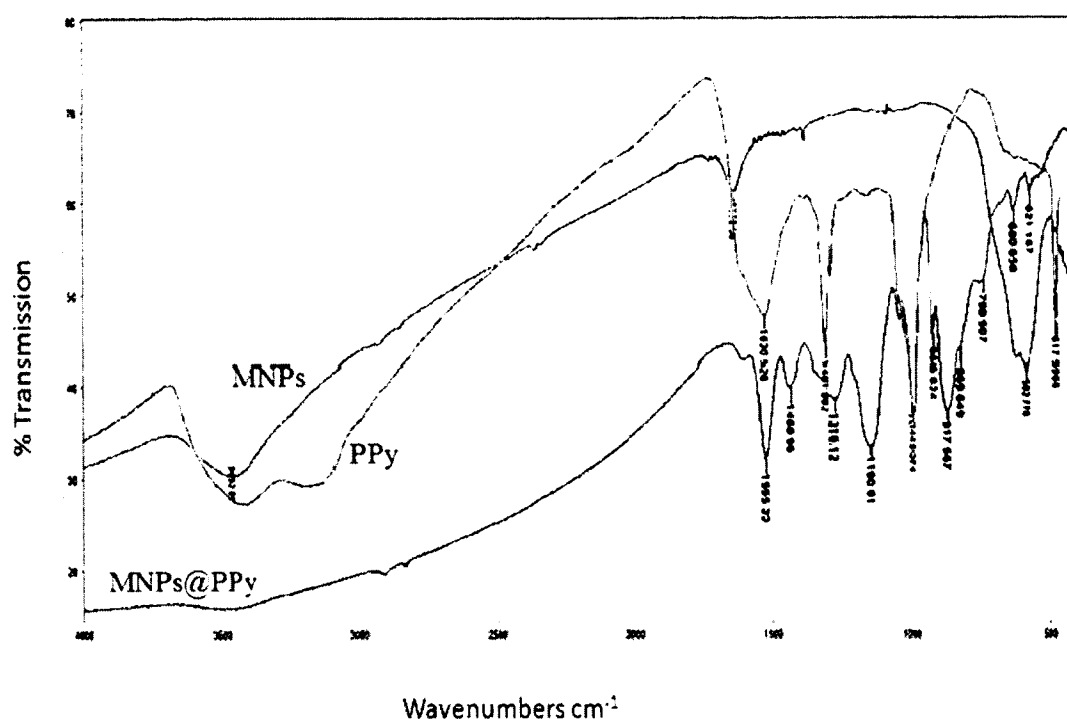
Figure 4.1 (a) FTIR spectra of MNPs, PPy and MNPs@PPy particles in KBr discs.

Figure 4.1(b) shows the FTIR spectra of MNPs and MNPs@PDA. After coating with polydopamine, some new bands appear at the range of 1626-816 cm^{-1}, and two characteristic peaks at 2919 cm^{-1} and 2851 cm^{-1} observed for PDA. The adsorption at about 1626 cm^{-1} corresponds to superposition of N-H bending and phenylic C=C stretching of PDA (lit., [79] 1609 cm^{-1}). Three bands at 1467, 1386 and 1223 cm^{-1} are related to N-H scissoring, phenolic O-H bending, and C-O stretching of PDA (lit., [79] 1510, 1350 and 1284 cm^{-1}) which proved the existence of polydopamine coating on MNPs surface.
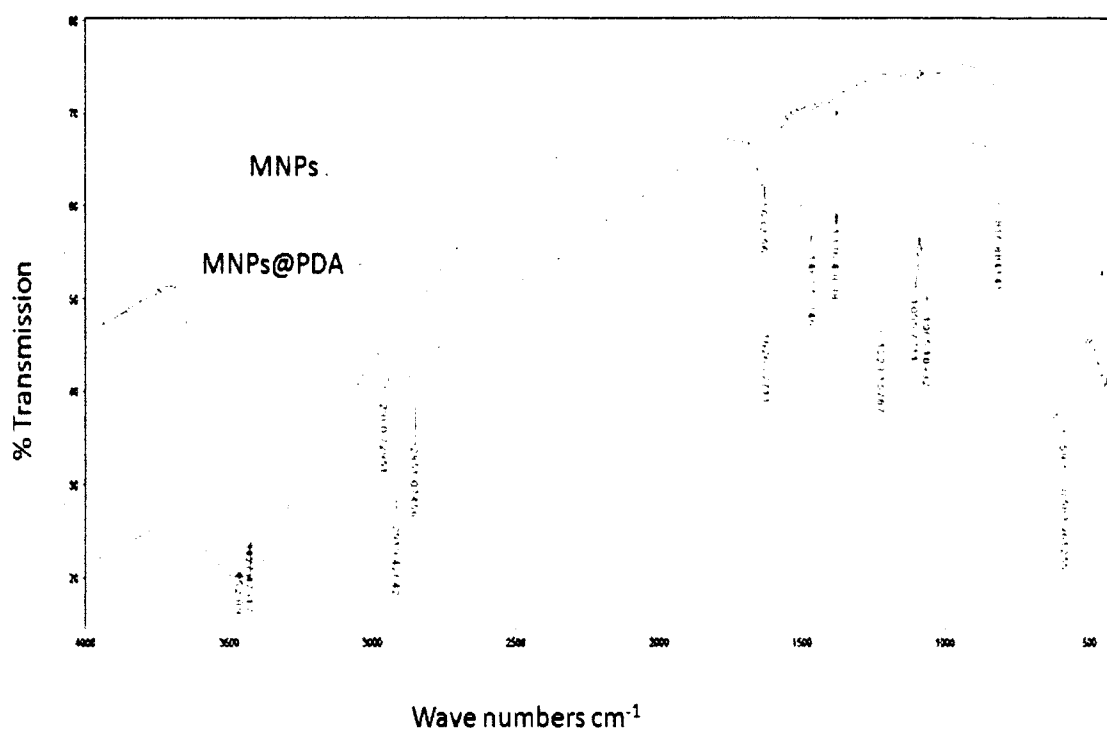
Figure 4.1 (b) FTIR spectra of MNPs and MNPs@PDA particles in KBr discs.

4.3 Characterization of MNPs, MNPs@PPy and MNPs@PDA particles' sizes

Scanning electron microscopy (SEM) was used to measure the particles' size and coating thickness. The SEM images of MNPs, MNPs@PPy and MNPs@PDA particles are shown in Figure 4.2(a) (b) (c). The average diameter (size) of MNPs, MNPs@PPy and MNPs@PDA particles were estimated to be 45-50, 70-75, and 75-80 nm respectively. The larger diameter of polymer-coated MNPs indicated that MNPs were successfully coated with polymer (PPy or PDA). The thickness of PPy and PDA coating were estimated to be 12-15 and 15-18 nm.

a) MNPs
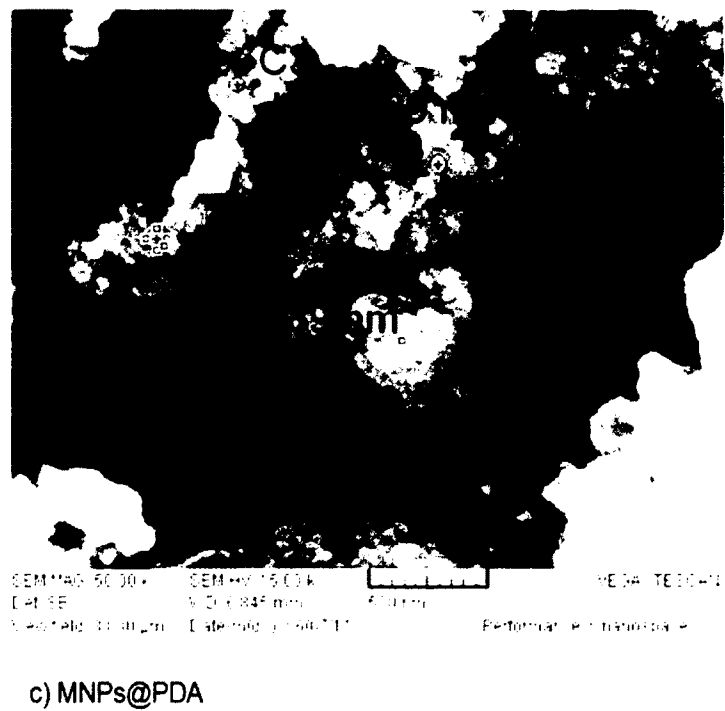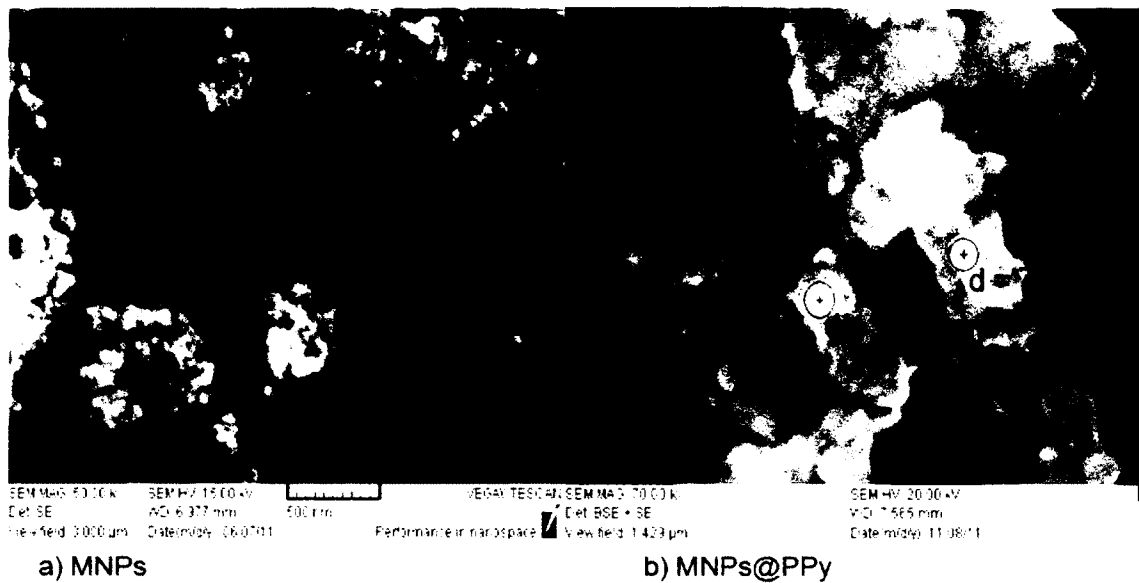
b) MNPs@PPy

c) MNPs@PDA

Figure 4.2 SEM images of (a) MNPs, (b) MNPs@PPy, and c)MNPs@PDA.

4.4 Thermogravimetric analysis of MNPs, PPy and MNPs@PPy particles

Thermogravimetric analysis of PPy and MNPs@PPy were conducted to investigate the stability of these particles and to confirm the tenacious interaction between MNPs and PPy. As shown in Figure 4.3,
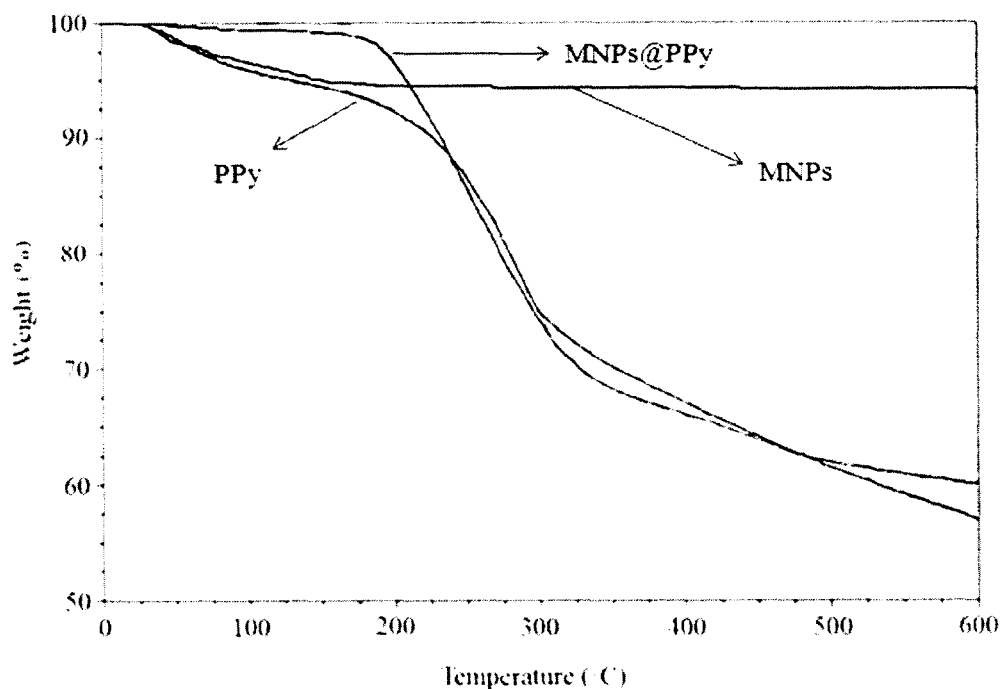
Figure 4.3 TGA curves of MNPs, PPy and MNPs@PPy particles.

MNPs@PPy followed a thermal decomposition profile (and gradual weight loss) similar to that for PPy particles. The onset temperature was determined to be 150 °C for PPy and 218 °C for MNPs@PPy. After coating with PPy, MNPs appeared to be more stable than PPy due to strong interactions between magnetic nanoparticles and polypyrrole molecular

chains. The initial weight loss of PPy, MNPs and MNPs@PPy below 100 °C was probably due to the removal of water [76].

Fast decomposition was observed beyond 225 °C in both MNPs@PPy and PPy. The residue percentages of MNPs, MNPs@PPy and PPy at 600 °C in nitrogen were 96, 62 and 57% which showed that polypyrrole is carbonized to form graphitic structures and cannot decompose entirely in nitrogen [80].

4.5 X-ray-diffraction and XPS Analysis

X-ray diffraction (XRD) is an efficient and non-destructive technique that provides detailed information about the chemical composition and crystal structure of materials. XRD analysis of the MNPs and MNPs@PPy was carried out to confirm the modification of MNPs by a coating of PPy. Figure 4.4 shows the XRD patterns of MNPs and MNPs@PPy. The peaks appearing at $2\theta = 31.7°$, $37.1°$, $44.8°$, $55.3°$, $58.9°$ and $64.4°$ were confirmed as MNPs. (lit., [81] $30.13°$, $35.57°$, $43.24°$, $53.82°$, $57.17°$, and $62.92°$, [82] $30.1°$, $35.4°$, $43.5°$, $53.4°$, $56.9°$, and $62.5°$). These characteristic peaks of MNPs represent the face-centered cubic lattice structure of Fe_3O_4 [80, 81]. A peak at $2\theta = 14.6°$ and a broad band at $22°$ are distinct peaks that indicate the modification of MNPs by PPy (lit., [81] 20-30°, [82] 24.2°). The characteristic peak at $2\theta = 22°$ is corresponding to the amorphous PPy which is caused by the scattering from their polymer chains at the interplanar spacing [81, 82]. This modification is also evidenced by a reduction in intensity of several PPy peaks in the MNPs@PPy spectrum.
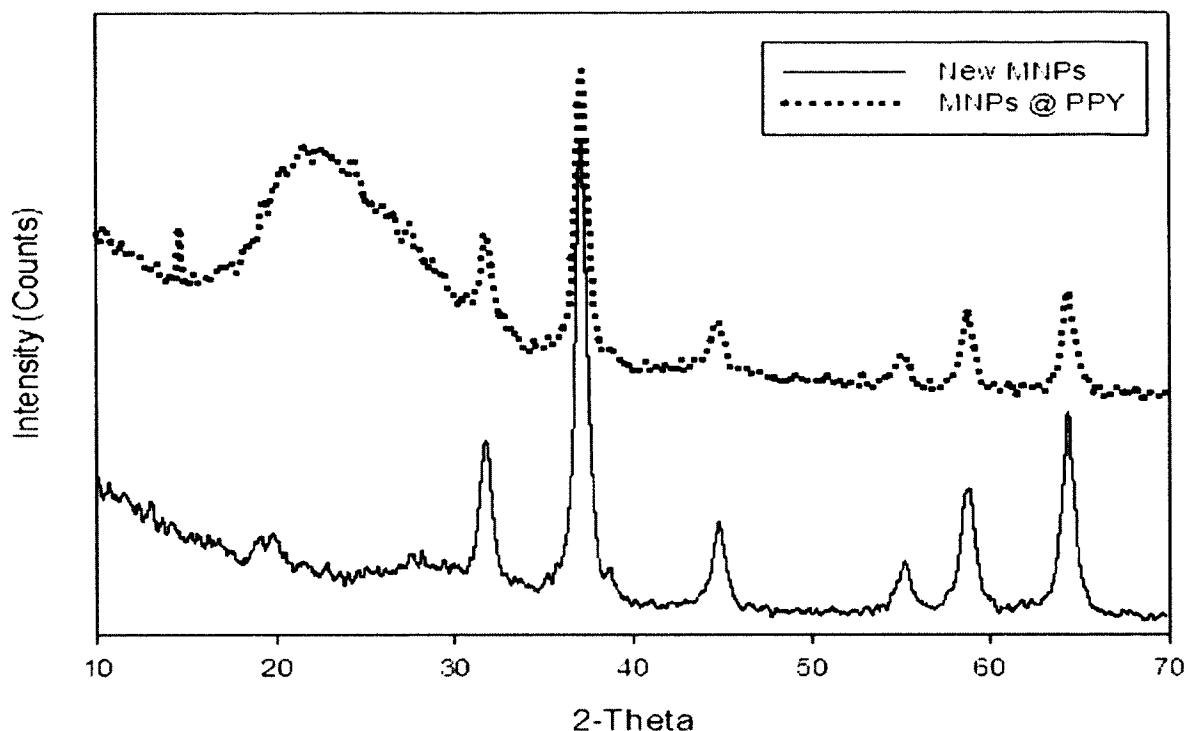
Figure 4.4 XRD spectra of MNPs and MNPs@PPy particles.

X-ray photoelectron spectroscopy (XPS) is a widely used surface analysis technique. It has been applied by many researchers to characterize the component on the surface of polymer-coated Fe_3O_4. The binding energy of Fe peak is about 702 - 730 eV and normally found to be absent on the surface of polymer-coated Fe_3O_4 [76]. Usually N atoms of PPy chains are divided into three different nitrogen species, such as the imine-like (=N-), amine-like (-NH-), and positively charged nitrogen (N^+) structures. Normally the N 1s core-level spectrum of PPy is deconvoluted into four peaks. The main peak at the binding energy of 399.8 eV is characteristic to the amine-like- (-NH-) structure. The peak at the binding energy of 398.6 eV is attributed to the imine-like (=N-) nitrogen species. Two other peaks with binding energy above 400 eV are related to the positively

37

charged nitrogen (N^+) structure [83]. The polymer coating can be calculated from the ratio of the peak area of N^+ to the total of N 1s. Generally the N^+ species is higher in PPy-coated MNPs due to the formation of $PPy-Fe_3O_4$ complexes. Since Fe is a transition metal, it can form coordination bond with –NH of PPy chains.

In comparison to MNPs with MNPs@PDA spectra, the original MNPs contains little carbon and nitrogen content, whereas MNPs@PDA contains peaks corresponding to C1s (284.5 eV) and N 1s (399.5 eV) as reported by Ren et al. [84]. They showed that their calculated nitrogen-to-carbon (N/C) ratio of the PDA-coated MNPs was close to the theoretical N/C (0.125) for dopamine.

4.6 In-capillary binding test

In recent years magnetic nanoparticles (MNPs) based on iron oxide, have attracted much interest thanks to their multifunctional properties, such as biocompatibility, superparamagnetism, small size and low toxicity [85]. The water-soluble Fe_3O_4 nanoparticles were applied by Wang et al. as adsorbents for heavy-metals removal from wastewater [86]. Water-soluble Fe_3O_4 nanoparticles showed high solubility (28 mg mL^{-1}), stability and exhibited excellent removal ability for heavy-metal ions (Pb^+ and Cr^+) from waste water. The most important advantage of applying Fe_3O_4 nanoparticles as adsorbents is that they can be easily separated from the reaction system with an external magnetic field. In this work, the binding ability of Fe_3O_4 nanoparticles was first investigated by an in-capillary binding test with three model pharmaceuticals (PF, MF, and QS) and three endocrine disrupting compounds (BPA, NAA, and TC) in water samples followed by an *in-vitro* binding test which will be discussed in the next section.

All analytes of interest (BPA, MF, NAA, PF, TC, and QS), MNPs, MNPs@PDA and MNPs@PPy particles were detected by UV light absorption at a common wavelength of 200 nm. CE is an instrumental method that can separate analytes on the basis of their difference in charge and size, inside a fused silica capillary filled with BGE, under a high electric field. CE-UV is also an attractive technique for rapid in-capillary binding tests because the amounts of compound and particles could be varied easily by controlling their injection times. Table 4.1 summarizes the electrophoretic mobility results calculated for the analytes and particles, which basically correspond to their charge-to-size ratio values. It can be concluded that MF and PF were positively charged in the BGE since they migrated faster than the neutral marker, MO. QS and BPA can be considered as neutral compounds since they migrated nearly the same as MO. The slow migration of TC indicates its negative charge in the BGE and similarly, NAA can be considered as even more negatively charged. In addition, late migration of MNPs, PDA-coated and PPy-coated MNPs implies their negative charge in the BGE as can be seen in Table 4.1.

Table 4.1 Electrophoretic mobility values of analytes, MNPs, MNPs@PDA and
MNPs@PPy particles in 20 mM Na_2HPO_4 BGE (pH 8.5 ± 0.2).

	Migration Time (min)	Molecular Weight (g.mol^{-1})	Electrophoretic Mobility (m^{2}V^{-1}s^{-1})
MNPs	7.8 ± 0.1	231.54	-2.21×10^{-8}
MNPs@PDA	8.2 ± 0.1	-----	-2.34×10^{-8}
MNPs@PPy	8.6 ± 0.1	-----	-2.46×10^{-8}
Bisphenol A (BPA)	4.5 ± 0.1	228.29	-2.91×10^{-9}
Mesityl Oxide (MO)	4.2 ± 0.1	98.14	00
Metformin (MF)	3.4 ± 0.1	165.62	1.18×10^{-8}
Naphthalene acetic acid (NAA)	6.9 ± 0.1	186.20	-1.87×10^{-8}
Phenformin (PF)	3.7 ± 0.1	205.26	6.94×10^{-9}
Triclosan (TC)	5.5 ± 0.1	289.54	-1.12×10^{-8}
Quinine sulfate (QS)	4.0 ± 0.1	782.96	2.78×10^{-9}

For in-capillary binding tests, MNPs, MNPs@PPy, or MNPs@PDA particles (suspended in BGE, 10 mg.mL^{-1}) were injected for 48 s (1st injection), and the analyte (dissolved in BGE, 200 μg.mL^{-1}) was next injected for 3 s. Quantification using our built-in-lab CE system was validated with mesityl oxide as an internal standard. Injection variation did not affect EDC and PPCP peak areas significantly even with nanoparticles in the capillary.

Table 4.2 summarizes in-capillary % binding test results of three kinds of nanoparticles with target compounds. The second column in Table 4.2 shows the in-capillary % binding results of MNPs. From in-capillary % binding results, it can be concluded that MNPs have poor binding efficiency with these target EDCs and PPCPs due to weak interaction. Therefore, surface modification of MNPs with a suitable polymer was necessary.

Table 4.2 In-capillary % binding of analytes with three different types of nanoparticles (10 mg.mL^{-1}) in 20 mM Na$_2$HPO$_4$ BGE (pH 8.5 ± 0.2). All % binding results are presented as mean ± standard deviation of triplicate measurement (n = 3).

Analytes (200 µg.mL^{-1})	% Binding with MNPs (10 mg. mL^{-1})	% Binding with MNPs@PDA (10 mg. mL^{-1})	% Binding with MNPs@PPy (10 mg. mL^{-1})
Bisphenol A (BPA)	5 ± 3	65 ± 5	99 ± 1
Metformin (MF)	2 ± 2	14 ± 6	34 ± 4
Naphthalene acetic acid (NAA)	7 ± 3	21 ± 4	39 ± 6
Phenformin (PF)	5 ± 3	99 ± 1	99 ± 1
Triclosan (TC)	6 ± 3	92 ± 3	99 ± 1
Quinine sulfate (QS)	8 ± 2	94 ± 2	98 ± 2

Surface modified MNPs have been widely used for many applications such as nanobiology, nanomedicine, and environmental science [21]. Usually, these applications need special surface coating to provide the MNPs particular functionality such as dispersibility, biocompatibility, fluorescence, and adsorption capacity. The coating principle can be based on covalent attachment, van der Waals interaction, and electrostatic interactions.

Polydopamine is an adhesive, multifunctional, and mussel-inspired biopolymer [87]. Biopolymers are usually found to be non-toxic, selective, efficient, inexpensive, and biodegradable [88]. Recently, in our lab, PDA-modified MNPs were applied for a rapid CE-UV binding test of *Escherichia coli* bacteria and environmentally hazardous compounds (BPA, proflavin, and NAA) [45, 57]. Hence, MNPs@PDA particles were next investigated by in-capillary binding test with these target EDCs and PPCPs. The third column in Table 4.2 summarizes the in capillary % binding results of MNPs@PDA. MNPs@PDA showed higher in-capillary % binding (92 to 99%) with TC, QS, and PF through π-π interaction of analytes and PDA. BPA exhibits moderately strong % binding (65%) with MNPs@PDA, whereas MF and NAA show poor binding (14-21%). These bindings can be explained by non-aromaticity of MF and weak interaction between the amino/imino/catechol functional groups (in PDA) and the carboxyl functional group in NAA.

Finally, MNPs@PPy particles were investigated by an in-capillary binding test with the above EDCs and PPCPs. Polypyrrole is one of the most studied conducting polymers that have high electrical conductivity, stability, and multi-functionalized applications [89, 90]. Polypyrrole coating possesses a highly π-conjugated structure and hydrophobicity.

Polypyrrole-coated sawdust (PPy/SD) was used by Ansari et al. for effective removal of organic dyes from textile wastewaters [91]. PPy has been used as a solid phase extraction material for the extraction of many organic compounds from a series of matrices due to formation of π-π complex and / or hydrophobic interactions between PPy and analytes [92-94]. Polypyrrole coated MNPs were employed as magnetic solid-phase extraction sorbents for extraction of estrogen from milk samples [95], and recently MNPs@PPy particles have been applied by Meng *et al.* to selectively preconcentrate seven phthalates in water samples [39]. Since most of the compounds (BPA, NAA, PF, TC, and QS) studied for this research possess an aromatic ring in their chemical structure, MNPs@PPy particles was a good candidate to investigate its binding efficiency with these aromatic compounds.

The last column in Table 4.2 summarizes the most prominent in-capillary % binding results of MNPs@PPy. Figure 4.5 represents the electropherograms of standard BPA, PF, TC and NAA in BGE and Figure 4.6 demonstrates the electropherograms of BPA, PF, TC and NAA binding with MNPs@PPy nanoparticles. A decrease in the analyte peak area indicated binding with MNPs@PPy at a certain efficiency.
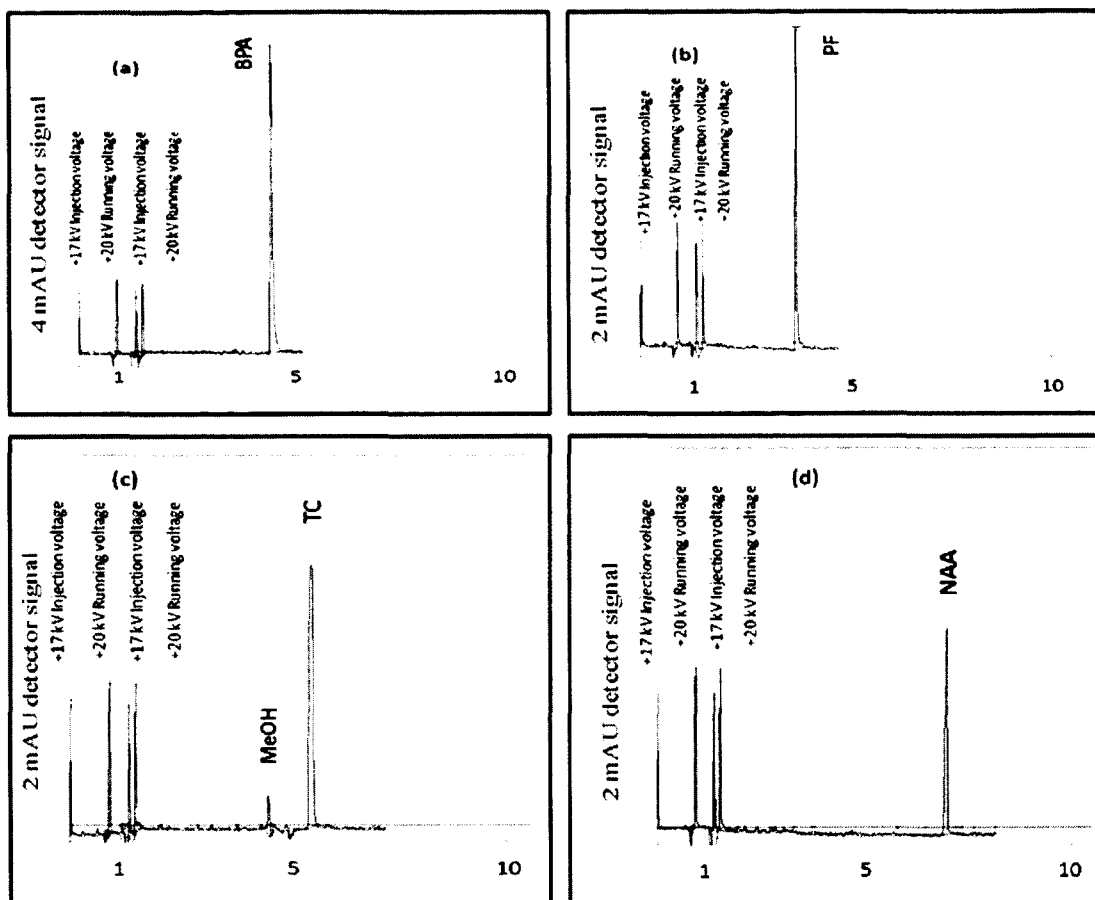
Figure 4.5 Electropherograms of standard BPA, PF, TC, and NAA in BGE. Electrokinetic injection at 17 kV: first 20 mM Na_2HPO_4 BGE for 48 s, and second target analytes (200 $\mu g.mL^{-1}$) in BGE for 3 s. (a) BPA, (b) PF, and (d) NAA. (c) TC (200 $\mu g.mL^{-1}$ in MeOH/BGE, 20:80 v/v). CE analysis at 20 kV; UV detection at 200 nm.
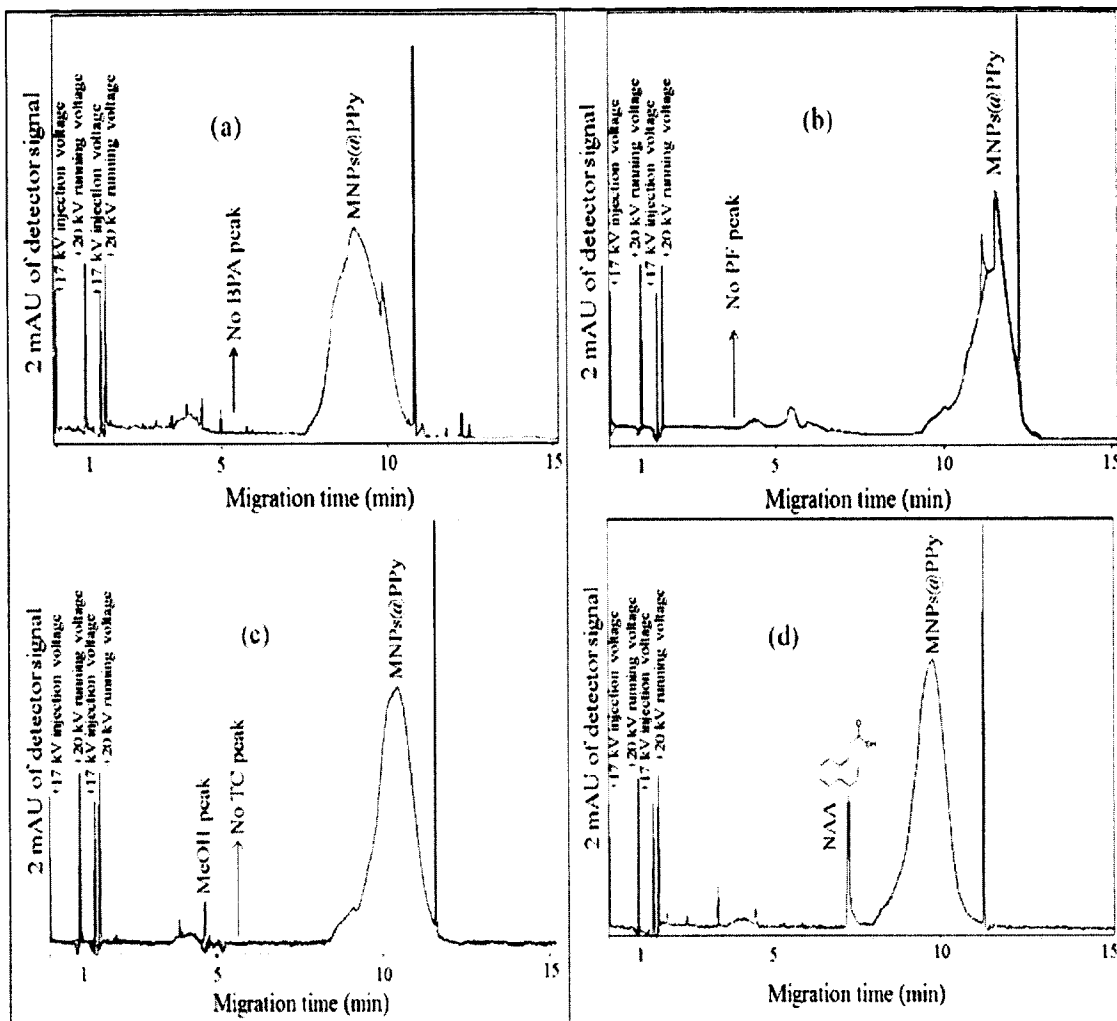
Figure 4.6 In-capillary CE-UV binding tests. Electrokinetic injection at 17 kV: first MNPs@PPy (10 mg.mL^{-1}) in 20 mM Na$_2$HPO$_4$ BGE for 48 s, and second target analytes (200 μg.mL^{-1}) in BGE for 3 s. (a) BPA, (b) PF, (c) TC, and (d) NAA. CE analysis at 20 kV; UV detection at 200 nm. The spike after the MNPs@PPy peak was of unknown origin.

Apparently, analyte compounds that have an aromatic ring in their molecular structures showed higher binding efficiencies, probably due to π-π bonding interactions and hydrogen bonding with PPy and analytes. It is important to note that two aromatic rings

fused along a common C-C bond (in NAA) is not as good as two aromatic rings separated by a C-C-C bond (in BPA) or C-O-C bond (in TC). These latter structures seem to be a better match to the C-C bond structure in PPy.

In comparison with MNPs@PDA, MNPs@PPy particles showed better % binding with aromatic compounds. For example, MNPs@PPy showed $99 \pm 1\%$ in-capillary binding efficiency with BPA, whereas MNPs@PDA was $65 \pm 5\%$ under the same conditions (injection time, applied voltage, and concentration). The possible reason could be hydrogen bonding between the -N- atoms in PPy and the -OH groups of BPA is strong. In addition, there are -OH groups in PDA that can repel the -OH groups of BPA which might result in lower % binding with MNPs@PDA.

4.7 Effects of MNPs@PPy particles, BGE concentration and binding selectivity

In order to attain the maximum binding efficiency in the in-capillary binding test, the concentration of MNPs@PPy particles must be optimized. Therefore, the concentration of MNPs@PPy particles was optimized by testing, in stages, from 0.25-10 mg.mL^{-1}. PF was used as a model analyte to investigate the effect of all concentrations of MNPs@PPy particles in the in-capillary binding test. MNPs@PPy particles were first injected for 48 s. Next, PF (200 µg.mL^{-1}) was injected for 3 s. The % binding of PF versus concentration of MNPs@PPy particles results are shown in Figure 4.7.
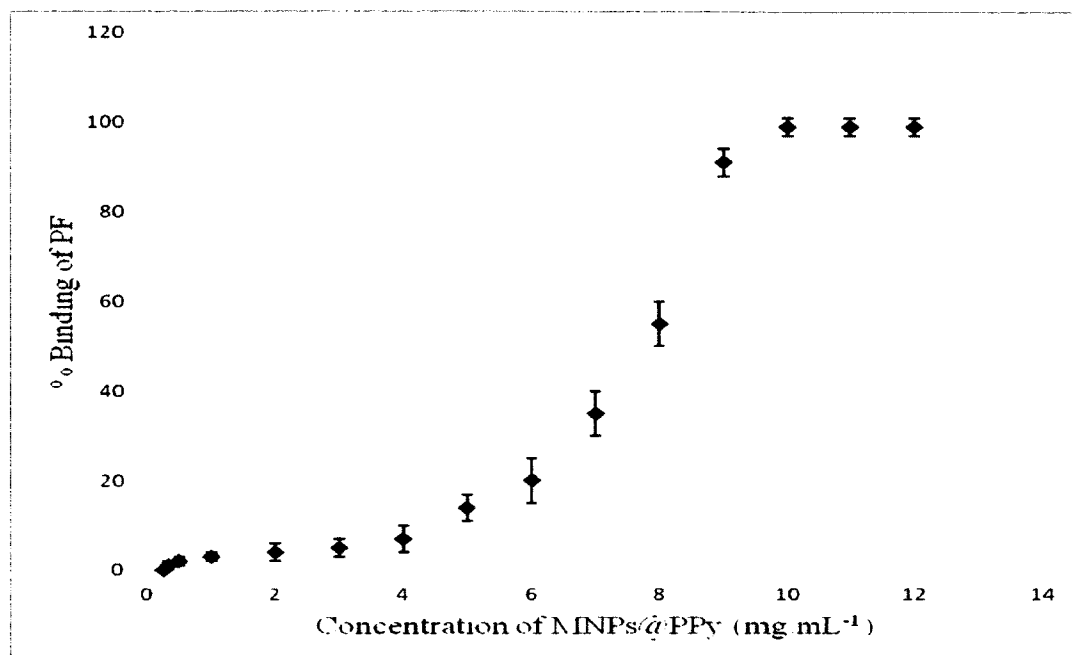
Figure 4.7 In-capillary % binding versus concentration of MNPs@PPy particles.

According to the graph in Figure 4.7, it can be seen that as the concentration of the particles decreases, the % binding of PF also decreases. Decreases in concentration reduce the number of the binding sites of MNP@PPy. From the experimental results, it was found that 10 mg.mL^{-1} of MNPs@PPy was the optimal concentration that provides maximum binding efficiency (as high as 99 ± 1%) with PF.

Two BGE concentrations (10 mM and 20 mM) were prepared at pH 7.5 ± 0.2 and 8.5 ± 0.2 to conduct in-capillary binding tests. Experimental results demonstrated similar in-capillary % binding results for both concentrations (10 mM and 20 mM BGE). It was observed that using 20 mM BGE (pH 8.5 ± 0.2) increased dispersibility of MNPs@PPy particles as well as increased electroosmotic flow (EOF) of the capillary. Higher EOF leads to analyte being detected at shorter migration time. This eventually helps to reduce the total analysis time.

In order to illustrate the binding selectivity of MNPs@PPy particles towards organic compounds, mesityl oxide (MO) was introduced as a control. MO's molecular structure does not contain an aromatic ring. PF was chosen as a model organic compound. MNPs@PPy (10 mg.mL^{-1}) particles were first injected for 48 s, then PF (200 μg.mL^{-1}), and MO (0.1% v/v) were in the second and third injection for 3 s. The experimental results revealed that MNPs@PPy particles selectively bind with PF (as high as 99 ± 1 %) leaving MO unchanged. Figure 4.8 shows the electropherograms of standard PF (200 μg.mL^{-1}), and MO (0.1% v/v) in 20 mM Na$_2$HPO$_4$ BGE and after binding with MNPs@PPy particles (10 mg.mL^{-1}) in BGE.
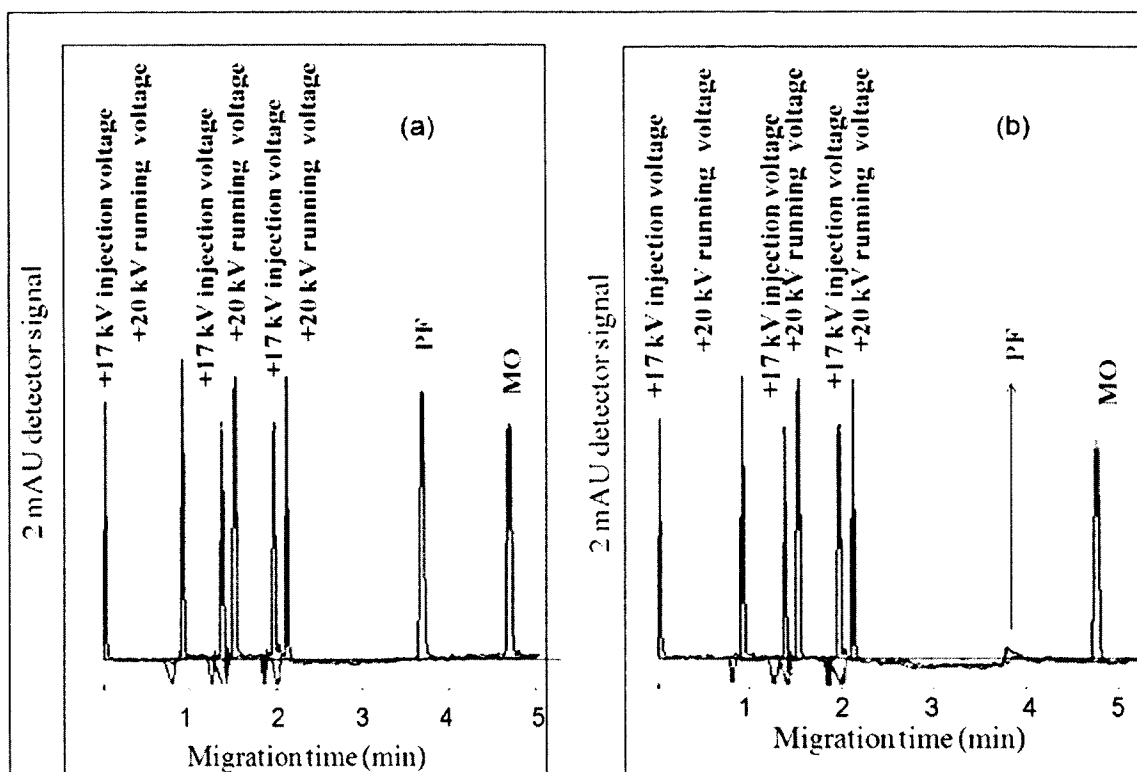
Figure 4.8 In-capillary CE-UV binding tests. Electrokinetic injection at 17 kV: (a) first

20 mM Na_2HPO_4 BGE for 48 s, second PF (200 $\mu g.mL^{-1}$) in BGE for 3 s. and

third MO (0.01% v/v) in BGE for 3 s. (b) MNPs@PPy particles in 20 mM

Na_2HPO_4 BGE (10 $mg.mL^{-1}$), second PF (200 $\mu g.mL^{-1}$) in BGE for 3 s and

third MO (0.1% v/v) in BGE for 3 s. CE analysis at 20 kV; UV detection at

200 nm. The MNPs@PPy peak is not shown in the electropherogram.

4.8 *In-vitro* **binding test**

In order to compare % binding in a competitive environment, a mixture of BPA, MF, NAA, PF, TC, and QS were used for *in-vitro* binding test. Figure 4.9 shows the electropherogram of the mixture of analytes in BGE.
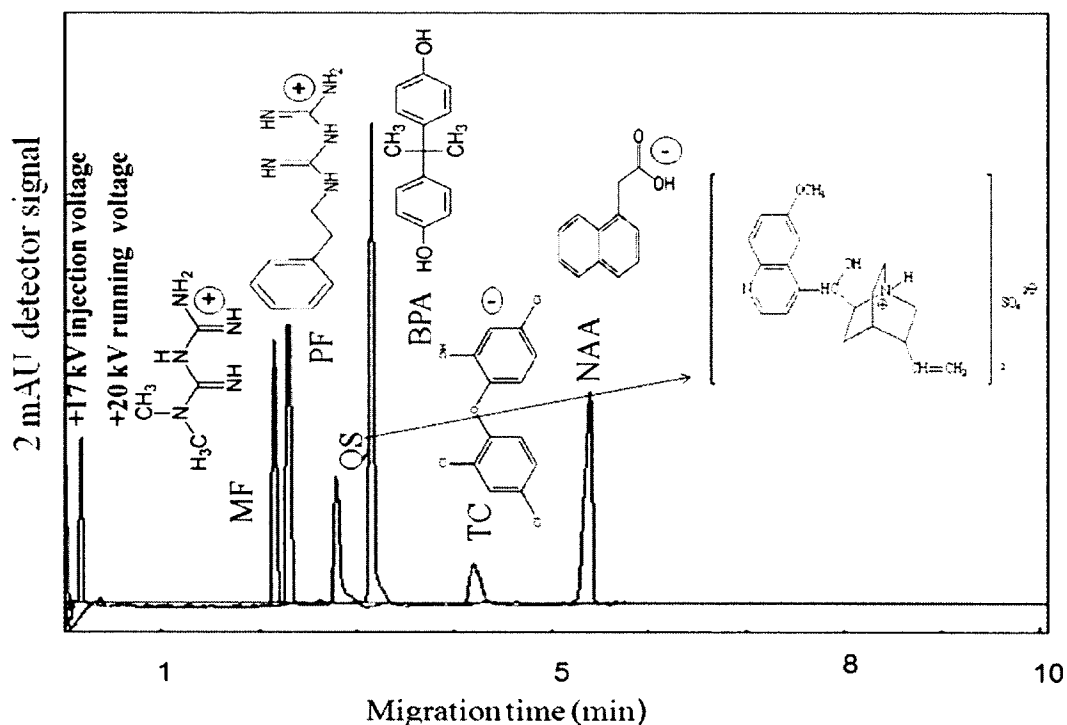
Figure 4.9 CE-UV electropherogram for a mixture of BPA, MF, NAA, PF, TC, and QS

(200 µg.mL^{-1}) in 20 mM Na$_2$HPO$_4$ BGE. Electrokinetic injection at 17 kV

for 3 s. CE analysis at 20 kV; UV detection at 200 nm.

The mixture was sequentially extracted for 10 min with one of three different particles (MNPs, or MNPs@PDA, or MNPs@PPy) and the supernatant was analyzed by CE-UV. Figure 4.10 shows the electropherogram of remaining analytes in the supernatant after extraction with unmodified MNPs. By comparing the peak areas before and after, the % binding was determined.

50

Figure 4.10 CE-UV electropherogram of remaining BPA, MF, NAA, PF, TC and QS in supernatant (20 mM Na_2HPO_4) after *in-vitro* extraction by MNPs (9 mg. mL^{-1}). Electrokinetic injection at 17 kV for 3 s. CE analysis at 20kV; UV detection at 200 nm.

From the electropherogram in Figure 4.10, it is seen that analytes peak area and intensity in supernatant didn't change significantly after extraction with MNPs. This indicates only (5-10%) binding efficiency for all analytes. The *in-vitro* % binding results of MNPs also agree with in-capillary % binding results.

Table 4.3 *In-vitro* % binding of analytes with three different nano particles (9 mg.mL^{-1})

in 20 mM BGE (pH 8.5 ± 0.2). All % binding results are presented as mean ±

standard deviation of triplicate measurement (n = 3).

Analytes (200 μg. mL^{-1})	% Binding with MNPs (9 mg. mL^{-1})	% Binding with MNPs@PDA (9 mg.mL^{-1})	% Binding with MNPs@PPy (9 mg.mL^{-1})
Bisphenol A (BPA)	10 ± 3	71 ± 5	94 ± 2
Metformin (MF)	5 ± 2	43 ± 3	30 ± 4
Naphthalene acetic acid (NAA)	8 ± 2	22 ± 2	68 ± 4
Phenformin (PF)	6 ± 3	94 ± 2	99 ± 1
Triclosan (TC)	7 ± 3	95 ± 1	99 ± 1
Quinine sulfate (QS)	10 ± 2	95 ± 1	99 ± 1

The electropherograms of remaining analytes in the supernatant after extraction with MNPs@PDA and MNPs@PPy particles are shown in Figures 4.11 and 4.12. The *in-vitro* % binding results of MNPs@PDA and MNPs@PPy are presented in the 3rd and 4th columns in Table 4.3. The *in-vitro* % binding results of MNPs@PDA and MNPs@PPy agree with the in-capillary % binding results (Table 4.2) with two exceptions. One exception was NAA which had a higher *in-vitro* % binding (68 ± 4%) compared to in-capillary (39 ± 6%) for MNPs@PPy particles. Secondly, MF showed higher *in-vitro* % binding (43 ± 3%) compared to in-capillary (14 ± 6%) for MNPs@PDA particles.

It is plausible that both *in-vitro* (a) NAA binding with MNPs@PPy, and (b) MF binding

with MNPs@PDA were controlled by slow kinetics. In both *in-vitro* tests, the interaction

time for analytes was significantly higher than in-capillary test which resulted in higher

% binding. MF showed the lowest binding efficiency for MNPs@PPy, as confirmed by

both in-capillary and *in-vitro* tests, due to a lack of aromatic ring in its molecular

structure. The 30% and 34% bindings were mostly the result of hydrophobic interaction

between MF and PPy.
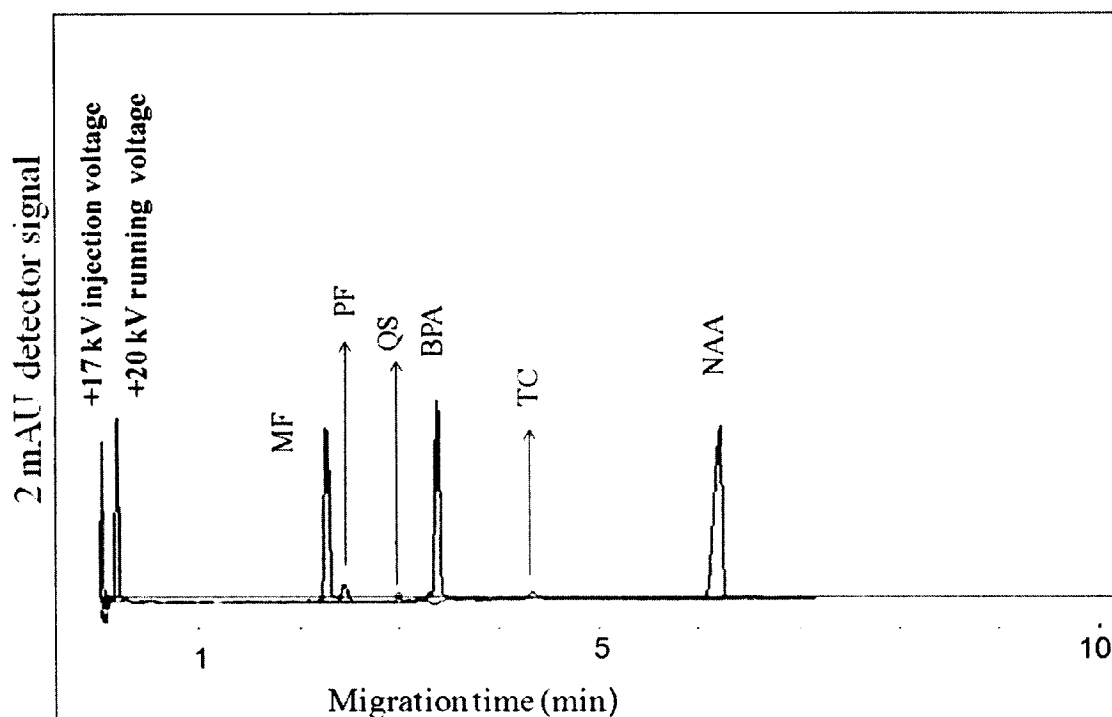
Figure 4.11 CE-UV electropherogram of remaining BPA, MF, NAA, PF, TC and QS in

supernatant (20 mM Na₂HPO₄) after *in-vitro* extraction by MNPs@PDA (9

mg.mL⁻¹). Electrokinetic injection at 17 kV for 3 s. CE analysis at 20kV;
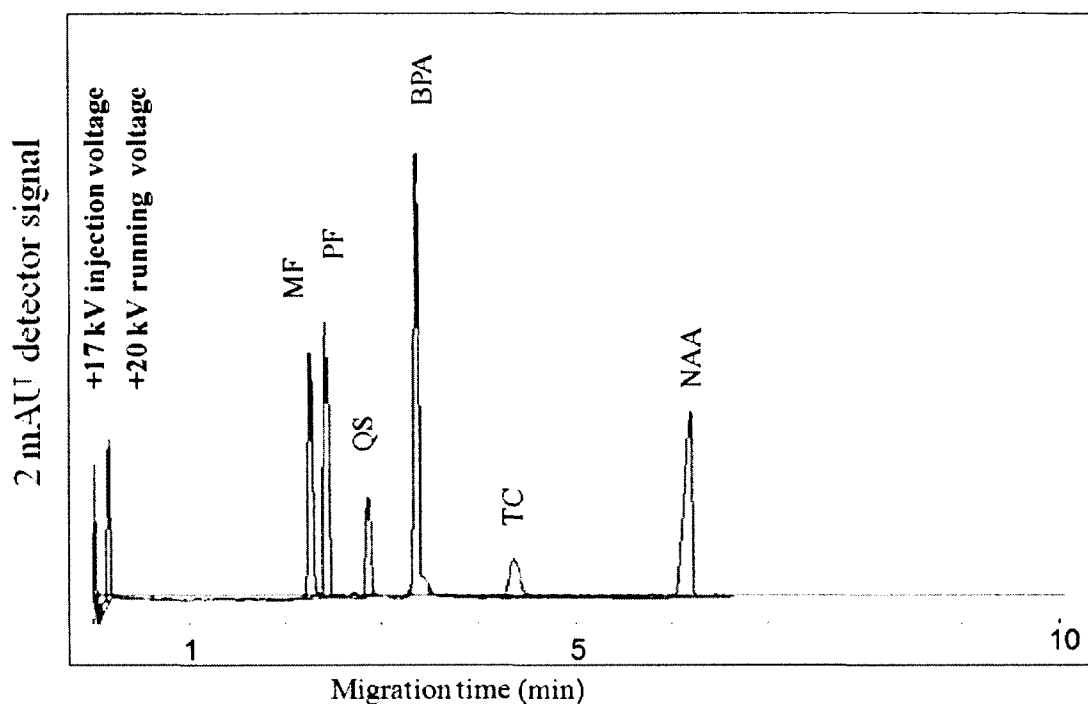
UV detection at 200 nm.
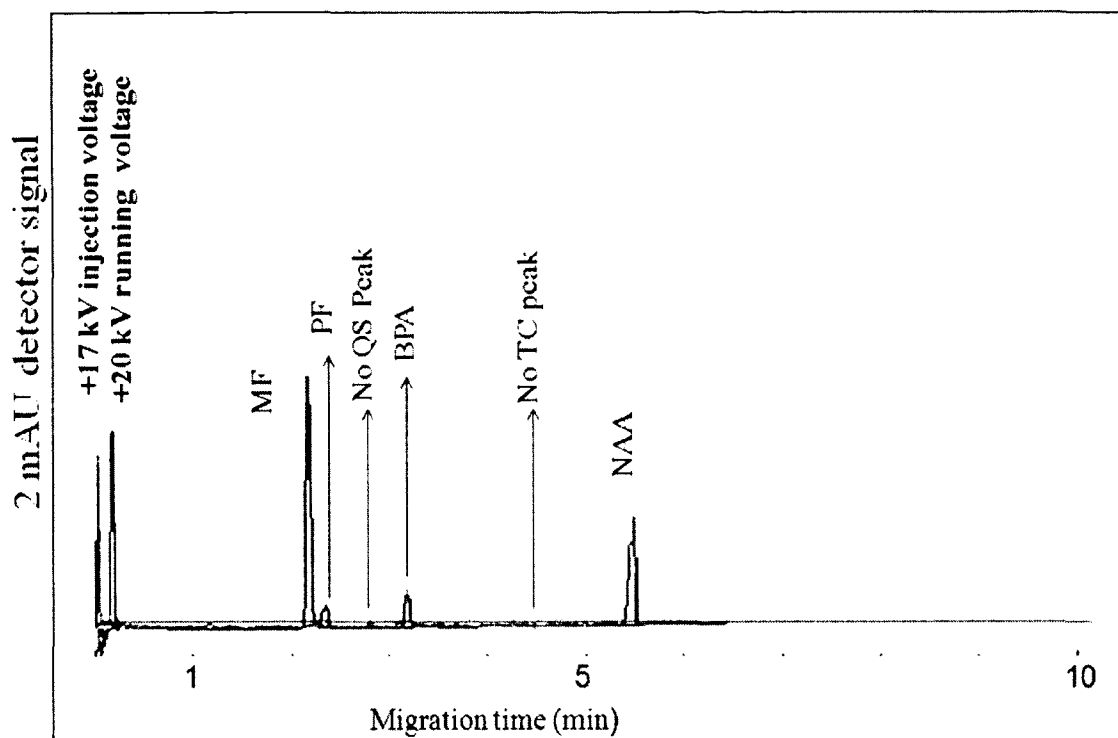
Figure 4.12 CE-UV electropherogram of remaining BPA, MF, NAA, PF, TC and QS in supernatant (20 mM Na_2HPO_4) after *in-vitro* extraction by MNPs@PPy (9 $mg.mL^{-1}$). Electrokinetic injection at 17 kV for 3 s. CE analysis at 20kV; UV detection at 200 nm.

Experimental results showed that MNPs@PPy was more selective and efficient in interaction with aromatic compounds (BPA, PF, TC, and QS) than non-aromatic compounds (MF and MO). Selectivity was assessed through in-capillary and *in-vitro* binding tests. Both binding tests showed a high % binding towards BPA, PF, TC and QS (as high as 99%), whereas non-aromatic compounds such as MF showed only 30%-34%.

Among three particles, MNPs, MNPs@PDA and MNPs@PPy, MNPs@PPy had higher binding capacity with aromatic compounds (BPA, PF, TC, and QS). This was due to their

porous structure and multifunctional properties. MNPs@PPy can be applied as a magnetic sorbent for the preconcentration of aromatic compounds (BPA, PF, TC, and QS) in future water analysis. In order to achieve the maximum extraction efficiency at a minimal cost, the amount of adsorbents (MNPs, or MNPs@PDA or MNPs@PPy) were optimized. It was determined that 9 mg of adsorbents offered the highest extraction efficiency for the target analytes.

4.9 Adsorption kinetics and Adsorption isotherms

Adsorption kinetics (based on the half-width of MNPs@PPy peak and the migration velocity of each analyte compounds relative to MNPs@PPy) provided an estimation of their overlap time to be in the range of 14.7-42.4 s, which was long enough to approach binding equilibrium.

The adsorption behavior of MNPs@PPy towards BPA, PF and TC was studied at room temperature. These analytes showed high % binding results from both in-capillary and *in-vitro* tests. Both the Langmuir and Freundlich equations were employed to plot the adsorption isotherms. The Langmuir equation can be written as $X/m = X_m b C_f + b C_f$ and the linear form of the Langmuir isotherm can be rearranged as:

$$m/X = 1/X_m + 1/ X_m b C_f$$

where X/m is the amount of analyte adsorbed by MNPs@PPy ($\mu mol.g^{-1}$), X_m is the maximum amount of analyte adsorbed ($\mu mol.g^{-1}$), C_f is the final concentration of analyte ($\mu mol.L^{-1}$) at equilibrium, and b ($L.\mu mol^{-1}$) is a Langmuir constant signifying the energy of sorption.

Similarly, the Freundlich equation can be presented as $X/m = KC_f^{1/n}$ and the linear form of the equation is $\log X/m = \log K + 1/n \ \log C_f$. Where K (μmol.g^{-1}) and $1/n$ are Freundlich's constants indicating adsorption capacity and intensity of adsorption, respectively [69]. Usually, a plot of $\log(X/m)$ versus $\log C_f$ is plotted for Freundlich isotherm and produces a straight line where n and K can be calculated (slope = $1/n$, and intercept = $\log K$).

The plot of m/X versus $1/C_f$ in Figure 4.13(a) shows how well the adsorption data was fitted to the Langmuir isotherm model. Reasonably high correlation coefficients were obtained for all three analytes, implying strong interactions of MNPs@PPy with BPA, PF and TC. The essential characteristics of Langmuir equation can be illustrated by the dimensionless equilibrium parameter $R_L = 1/(1+b.C_o)$, where C_o is the initial concentration of analytes (μmol.L^{-1}). The R_L value implies that the isotherm is unfavorable ($R_L > 1$), linear ($R_L = 1$), favorable ($0 < R_L < 1$), or irreversible ($R_L = 0$). R_L values of this experiment were all found to be favorable.

$y = 0.1504x + 0.0055$
$R^2 = 0.9561$

$y = 0.1463x + 0.0051$
$R^2 = 0.9629$

$y = 0.119x + 0.0032$
$R^2 = 0.9544$

m/X

1/C$_f$

◆ TC
■ BPA
▲ PF
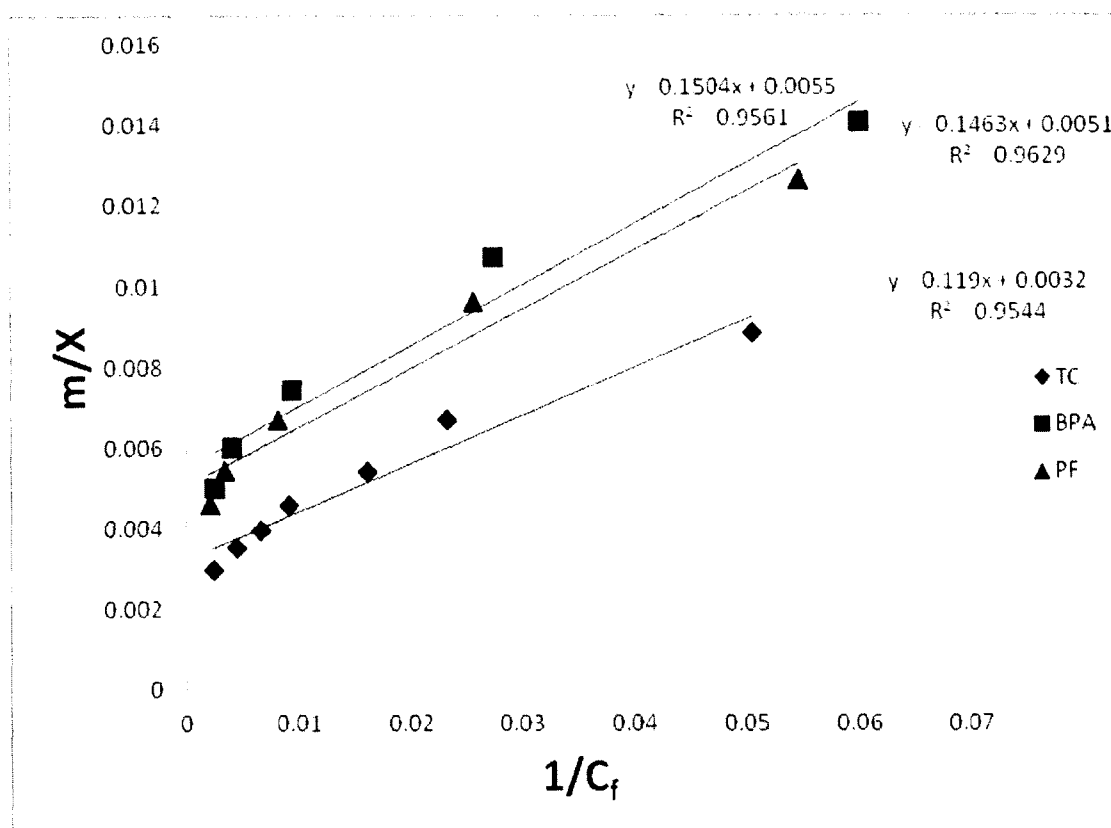
Figure 4.13 (a) Langmuir isotherms for adsorption of BPA, PF and TC by MNPs@PPy particles. BGE: pH 8.5 ± 0.2, agitation: 1500 rpm for 20 min, and sorbent dosage: 9.0 mg.mL^{-1}.

The Freundlich isotherms (log X/m versus log C$_f$) are shown in Figure 4.13(b). It is also noticeable that the adsorption isotherms of BPA, TC and PF fit well to the Freundlich model as high correlation coefficients were obtained for all three analytes. The maximum correlation coefficient obtained for TC ($R^2 = 0.9954$) indicates that the removal of TC using MNPs@PPy fits better with the Freundlich model compared to the Langmuir model ($R^2 = 0.9544$).

$$y = 0.3699x + 1.5788$$
$$R^2 = 0.9954$$

$$y = 0.2466x + 1.6206$$
$$R^2 = 0.9626$$

$$y = 0.2359x + 1.6700$$
$$R^2 = 0.9663$$

Log(X/m)

Log C_f

◆ TC
■ BPA
▲ PF
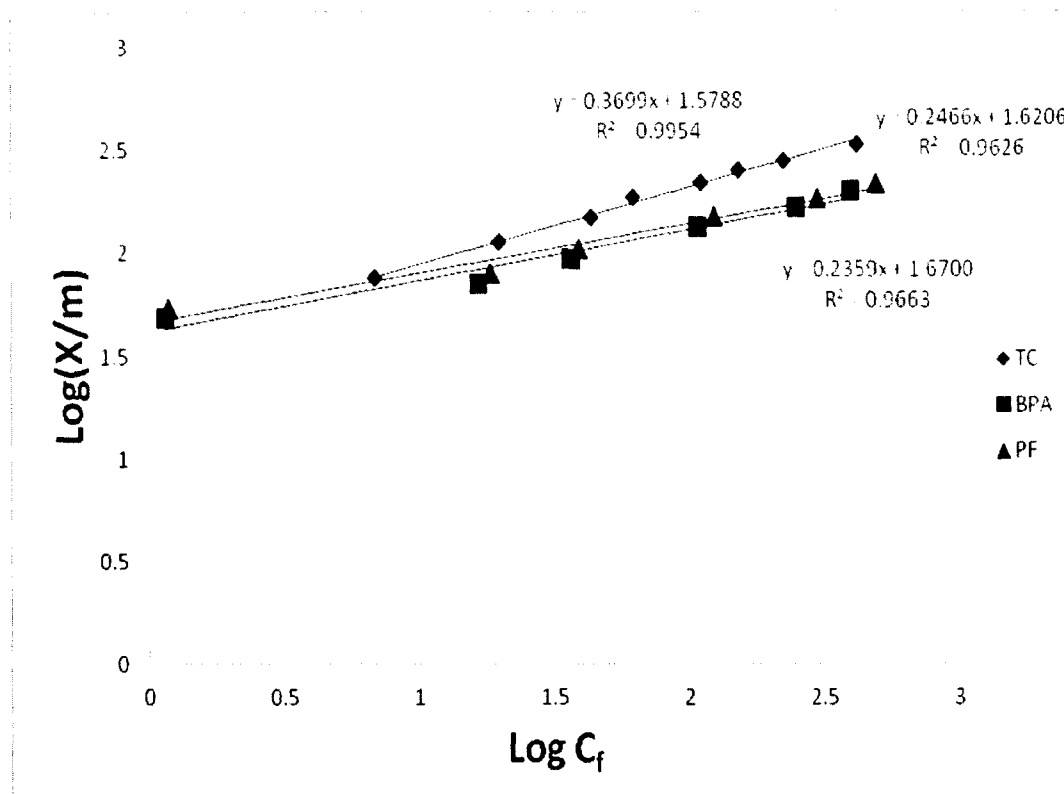
Figure 4.13 (b) Freundlich isotherms for adsorption of BPA, PF and TC by MNPs@PPy particles. BGE: pH 8.5 ± 0.2, agitation: 1500 rpm for 20 min, and sorbent dosage: 9.0 mg.mL⁻¹.
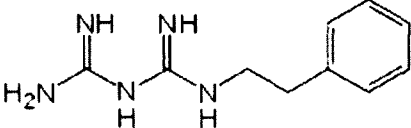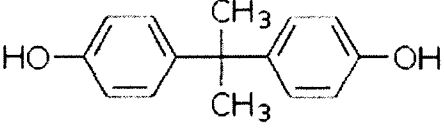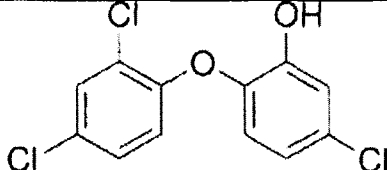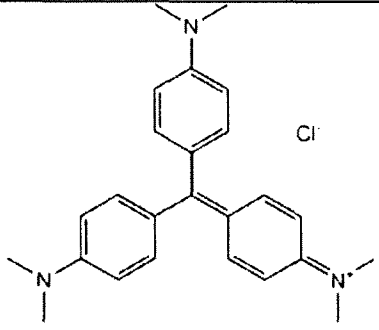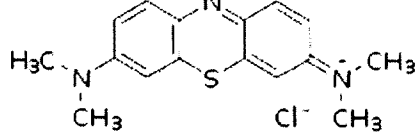
On the basis of slopes and intercepts of the straight lines, Langmuir and Freundlich constant values derived from these straight lines are presented in Table 4.4. The higher adsorption capacity (X_m) obtained for TC (312 $\mu mol.g^{-1}$) using the Langmuir model, implies a higher sorption capacity and better performance of MNPs@PPy adsorbent for removal of TC from aqueous solution. The higher value of K for PF, BPA, and TC from the Freundlich isotherms also indicates the higher affinity of MNPs@PPy towards these compounds. Freundlich's constant (n) values calculated for the three adsorbates indicate favorable adsorption. The n value of a favorable adsorption should be in the range of 1 to 10 [96].
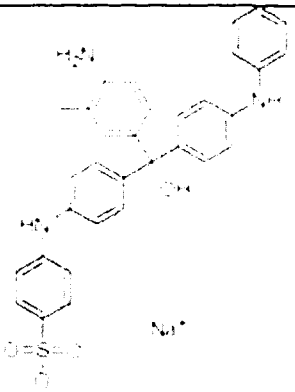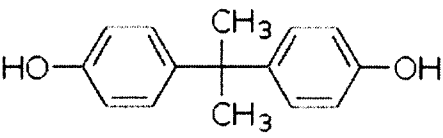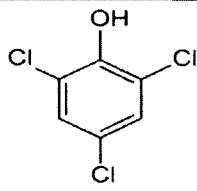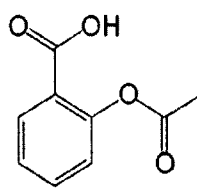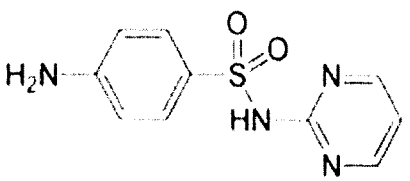
Table 4.4 Freundlich and Langmuir constant values obtained for three target compounds.
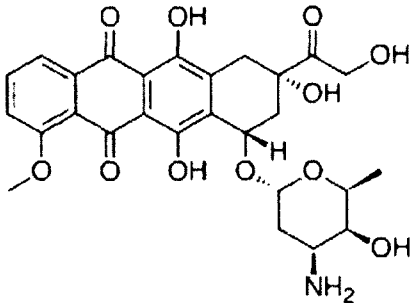
Adsorbate	n	K (μmol.g^{-1})	B (L.μmol^{-1})	X_m (μmol.g^{-1})
PF	4.24 ± 0.01	47 ± 2	0.035 ± 0.001	196 ± 3
BPA	4.05 ± 0.01	42 ± 2	0.036 ± 0.001	183 ± 2
TC	2.70 ± 0.01	38 ± 2	0.027 ± 0.001	312 ± 2

The maximum adsorption capacity (X_m) results of MNPs@PPy towards BPA, PF and TC were found to be high. They predicted a good performance of MNPs@PPy particles for the efficient removal of these aromatic compounds from aqueous solution. Bhaumik *et al.* had reported that PPy-coated Fe_3O_4 magnetic nanocomposite showed adsorption capacity of 169-243 mg.g^{-1} for Cr(VI) [97]. The BPA adsorption capacity on chitosan/fly-ash-cenospheres/γ-Fe_2O_3 magnetic composites, as reported by Pan *et al.* was slightly less (32 mg.g^{-1}) in comparison to our MNPs@PPy (42 mg.g^{-1}) [98].

Table 4.5 Langmuir constant values obtained for MNPs@PPy in comparison with MNPs coated with various polymers.

Analyte	M.W. (g.mol⁻¹)	Molecular Structure	Particles Size (nm)	b (L.µmol⁻¹)	X_m (µmol.g⁻¹)	Reference
PF	205.3			0.035±0.001	196±3	
BPA	228.3		MNPs@PPy 70-75	0.036±0.001	183±2	This work
TC	289.5			0.027±0.001	312±2	
Crystal violet	408.0		Fe₃O₄@APS @AA-*co*-CA 15-20	0.045	510	[99]
Methylene blue	319.8			0.060	400	

Compound	MW	Structure	Adsorbent			Ref.
Alkali blue 6B	612.7			0.009	40	
BPA	228.3		Chitosan/fly-ash cenospheres/ γ-Fe_2O_3 140000	0.001	342	[98]
2,4,6-trichlorophenol	197.5			0.001	539	
Aspirin	180.2		Polymerized -glucose coated Fe_3O_4 magnetic nanoparticles 40-220	-	1277	[100]
Sulfadiazine	250.3		Molecularly imprinted Fe_3O_4@SiO_2 magnetic nanoparticles 300	-	60	[71]

Name	MW	Structure	Nanoparticle			Ref
Doxorubicin	543.5		Fe$_3$O$_4$-CMC-AA-FA nanoparticles 25±5	-	684	[101]
Lysozyme	13400		Fe$_3$O$_4$@NIPDA 22.5-47.5	0.10	9.7	[75]
Bovine Serum Albumin	68000			1.1	0.9	
Trypsin	23300			0.39	2.6	
Bovine Hemoglobin	64500			0.46	2.2	
Cytochrome C	12400			0.62	1.6	
Bovine serum albumin	68000		Fe$_3$O$_4$@Poly arginine 10.4±2.36	1.6	0.63	[102]
α-Lact-albumin	14178			0.4	2.5	
Carbonic Anhydrase	29000			2.0	0.5	
Myoglobin	17800			5.1	0.2	
Cytochrome C	12400			1.5	0.7	
Lysozyme	13400			5.3	0.2	
Plasmid DNA	1946000		Poly(hydroxyethyl methacrylate -N-	-	0.08	[103]

			methacryloyl -(L)- histidine) coated Fe$_3$O$_4$ 91.5			
Cd^{2+}	112.4		3-	0.058	264	
Zn^{2+}	65.4		Aminopropy	0.004	668	[30]
Pb^{2+}	207.2		ltriethoxysila	0.029	802	
Cu^{2+}	63.5		ne copolymers of acrylic/croto nic acid modified Fe$_3$O$_4$ 15-20	0.002	1995	

Fe$_3$O$_4$@APS@AA-*co*-CA : Fe$_3$O$_4$ modified with 3-aminopropyltriethltriethoxysilane and copolymers of acrylic acid and crotonic acid.

Fe$_3$O$_4$-CMC-AA-FA : Fe$_3$O$_4$ modified with carboxymethyl chitosan, acrylic acid and folic acid.

Fe$_3$O$_4$@NIPDA : Non imprinted Fe$_3$O$_4$ modified with polydopamine.

Several binding capacity results were recovered from the recent literature for a variety of organic compounds, proteins, DNA and metal ions that interacted with MNPs coated with different polymers. After they were added into Table 4.5, it became obvious that these X$_m$ results for BPA, PF and TC all fell within the literature range. Apparently, three X$_m$ results calculated from this experiment were close to each other. The difference between TC and the other two compounds (BPA and PF) was relatively insignificant when compared to the large difference among the previously reported values. Aromatic

compounds exhibited comparable binding capacity results due to their similar hydrophobic interactions with the polymer-coated particles. The exception was for alkali blue 6B which has a higher M.W. than those of other aromatic compounds. The several X_m results for DNA and proteins (which are biomacromolecules) are very low, and those for metal ions are fairly high, mainly due to their extreme sizes.

4.10 Desorption test of MNPs@PPy particles

The % recoveries of target analytes from MNPs@PPy particles were also determined. A suitable solvent is necessary which can elute the adsorbed analytes from MNPs@PPy as much as possible. Meng et al. reported that EtAc gives the highest elution efficiency of phthalates from Fe_3O_4@PPy [39]. They also demonstrated that MeOH provides second highest elution efficiency of phthalates from Fe_3O_4@PPy. Only EtAc is not compatible in CE. Therefore, a mixture of ethyl acetate (EtAc) and MeOH (75:25, v/v) was selected as the eluting solvent. 2 mL of supernatant (eluting solvent) containing the desorbed analytes were collected for CE-UV analysis to determine all desorbed analytes. The % recoveries of bound analytes were found to be 85 ± 13% MF, 87 ± 13% PF, 54 ± 11% BPA, 52 ± 10 QS, 39 ± 11% TC and 37 ± 10% NAA. Except for MF and PF, these results were far from ideal for the preconcentration of analytes and regeneration of MNPs@PPy after each use.

4.11 Regeneration of MNPs@PPy particles

The addition of a new coating of PPy on the used particles (after binding with target analytes) was time saving and cost-effective way to recycle them instead of making new MNPs@PPy. The hypothesis was that this additional coating would be sufficient regeneration of the particle surfaces for binding more target analytes. Experimental results showed that the new PPy coating (after binding with BPA) regenerated the used MNPs@PPy particles for efficient binding with BPA again.
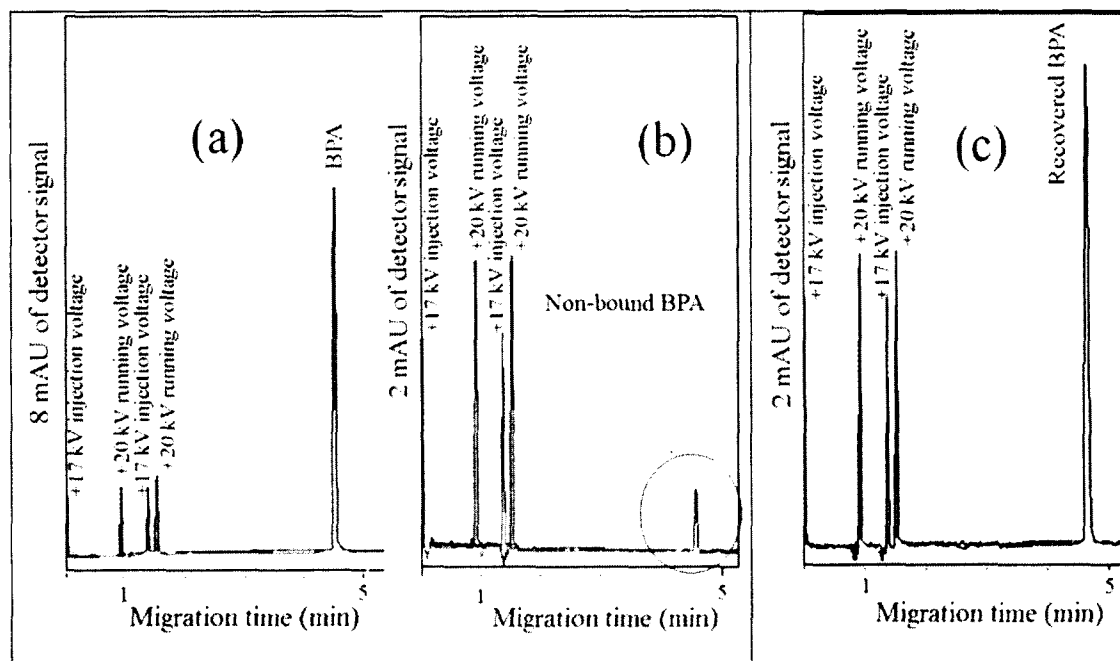
Figure 4.14 CE-UV electropherograms of BPA in (a) standard solution prepared in 20 mM Na₂HPO₄ BGE, (b) supernatant after extraction by regenerated MNPs@PPy particles, and (c) 20 mM BGE after EtAc and MeOH (75:25 v/v) elution and solvent evaporation. Electrokinetic injection at 17 kV: first 20 mM BGE for 48 s, and second the sample for 3 s. CE analysis at 20 kV; UV detection at 200 nm.

Figure 4.14 shows the electropherograms of BPA in three different stages of

evaluating the regenerated MNPs@PPy particles. These results demonstrated that the

% binding of BPA with regenerated MNPs@PPy particles was as high as 94 ± 3%,

and the % recovery of BPA by elution was determined to be 53 ± 4% of the bound

amount. Both results verified that the regenerated particles were functionally as good

as the original ones.

4.12 Application to river water analysis

The MNPs@PPy particles were applied to the analysis of a river water sample

collected from the Rideau River in Ottawa. A 0.22 μm filter was used to remove soil

particles contained in the river water. The filtrate was analyzed by CE-UV but none of

the analytes was found in a high enough concentration to be detectable by CE-UV.

Alternatively, background electrolyte (BGE) was prepared in the filtrate and then spiked

with phenformin. Then the spiked river water sample was tested by CE-UV for binding

with MNPs@PPy particles. The results showed that the binding efficiency of phenformin

in river water was 94 ± 4%. It was concluded that if the studied analytes were present in

detectable concentrations, the CE-UV technique would be able to validate how efficiently

MNPs@PPy particles removed them from the river water with minimal matrix effects.

Chapter 5

Conclusion

5.1 Conclusion

The demand for clean water supplies is rising with the growth in world population. It is one of the biggest challenges of the century to ensure a reliable clean water supply for every individual. The first step to ensure the access to safe drinking water would be protecting particularly fresh water, in its various sources including lakes, rivers and ground water. It is essential to stop throwing contaminants into these sources in order to protect environmental health. However, occurrence of pollutants is increasing as a result of more human activities and elevated quantities of wastes released into the environment. EDCs and PPCPs are constantly found in the environment from sources like sewage treatment plant effluent, agricultural runoff, concentrated animal feed, landfill leachates, as well as urban runoff. Cost effective practices for removal of EDCs and PPCPs will require both knowledge development and careful implementation.

Magnetic nanoparticles are currently attracting a wide range of applications in water treatment. Coating of MNPs with polydopamine and polypyrrole resulted in strong binding with aromatic compounds. In this study, MNPs, PDA-coated and PPy-coated MNPs were successfully synthesized and characterized. The selective binding properties of MNPs, MNPs@PDA and MNPs@PPy have been evaluated for efficient removal of different EDCs and pharmaceuticals (namely BPA, MF, NAA, PF, TC, and QS) by employing CE-UV as a rapid analytical technique. In-capillary and *in-vitro* binding tests were conducted for all three types of MNPs (unmodified MNPs, MNPs@PDA, and MNPs@PPy). High % binding (99 ± 1%) of MNPs@PPy with BPA, PF, TC, and QS were found due to π-π and hydrogen bonding interactions between PPy and analytes.

MNPs@PPy showed 94 - 99 % binding with BPA whereas MNPs@PDA was 65 - 71 % as confirmed by in-capillary and *in-vitro* binding tests.

Desorption test of MNPs@PPy particles were performed using a mixture of EtAc and MeOH (75:25, v/v) as eluting solvent. The % recoveries of the bound analytes were found to be between 87% and 37 %. Multiple coatings of PPy were being conducted to recycle the used particles. The new coating of PPy on the used particles proved to be time saving, cost effective and eluent free in recycling the used particles.

This work demonstrates how CE can be applied to analyze adsorption of EDCs and PPCPs by MNPs@PDA and MNPs@PPy. CE was a cost-effective method for analyzing the adsorption efficiency and elution recovery. In-capillary interaction was an interesting way to determine binding efficiency rapidly. In addition, adsorption isotherms of MNPs@PPy particles towards BPA, PF, and TC were also studied. The higher adsorption capacity (X_m) was obtained for BPA, PF, and TC demonstrated strong affinity and better performance of MNPs@PPy particles as adsorbents for efficient removal of these target organic compounds from aqueous solution.

5.2 Future work

Beside water treatment, magnetic nanoparticles are currently attracting a wide range of applications in medicine for drug delivery, diagnostic imaging, and therapeutic applications due to their small size and magnetic properties. They have been extensively evaluated for targeted delivery of pharmaceuticals through magnetic drug targeting [104]. Anticancer drugs are known to have side effects because of their lack of target specificity. Superparamagnetic iron oxide nanoparticles are found to be capable of carrying anticancer drugs into malignant cells while sparing healthy cells. They proved to be nontoxic with no treatment-related deaths [105, 106]. Magnetic nanoparticles have been conjugated with various anticancer drugs including paclitaxel, methotrexate, mitoxantrone, and doxorubicin to increase their target selectivity [107]. Loading of drug molecules onto the polymer-coated nanoparticles represents another approach of delivering drug to the target site. Amino-polyvinyl alcohol and pullulan-coated magnetic nanoparticles showed increase interaction of these nanoparticles with human cancer cells as well as reduction of cytotoxicity in healthy cells [108, 109].

In a recent study, superparamagnetic iron oxide nanoparticles and the anticancer drug, doxorubicin hydrochloride, were encapsulated into poly (D,L-lactic-co-glycolic acid) and poly(ethylene glycol) (PLGA-PEG) nanoparticles for local treatment [104]. Their magnetic properties helped to keep them in the patient's joint with an external magnet, thus rendering the cancer treatment very effective. It would be interesting research to evaluate MNPs@PPy particles as new carriers for anticancer drugs. X-ray photoelectron spectroscopy (XPS) can be done in future studies to analyze the PPy-coating surface of the particles.

MNPs@PPy particles strongly bind with pharmaceutical compounds such as PF and QS through aromatic interactions of analytes and polymer. Pharmaceutical compounds having an aromatic ring in their molecular structures showed binding selectivity towards MNPs@PPy particles. Previous *in-vitro* and in-vivo studies showed that polypyrrole is biocompatible with nerve tissue and non-toxic [110]. Common anticancer drugs including paclitaxel, methotraxate, mitoxantrone, and doxorubicin, all have aromatic rings in their molecular structures. Once their binding interactions with MNPs@PPy are rapidly confirmed by CE-UV analysis, these loaded particles would be a good candidate in future research for specific delivery of these drugs to target cancer cells.
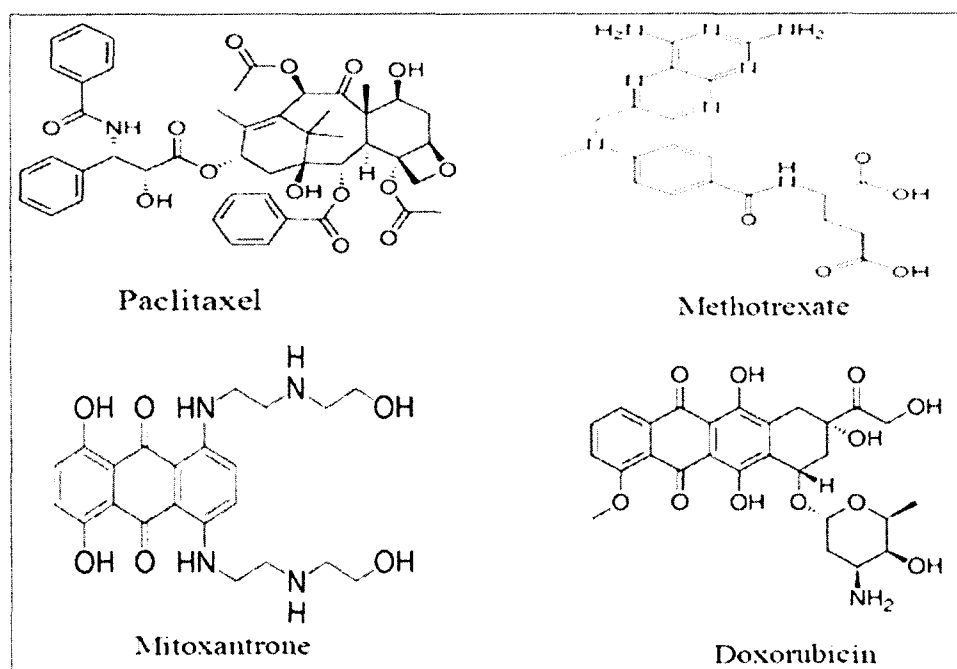

Figure 5.1 Chemical structures of paclitaxel, methotrexate, mitoxantrone, and doxorubicin [111].

References

[1] J. Hagerman, (May/June 2011). Quenching the world's thirst. *Lab Business*, p.18-20.

[2] X. Qu, J. Brame, Q. Li, and P. J.J. Alvarez, *Acc. Chem. Res.*, 2012, DOI 10.1021/ar300029v

[3] M. F. Rahman, E.K. Yanful, and S.Y. Jasim, *Desalination*, 2009, **248**, 578-585.

[4] J. P. Besse, and J. Garric, J. *Toxicol. Lett.*, 2008, **176**, p. 104-123.

[5] E. Loffredo, A. Traversa, and N. Senesi, *Ecotox. Environ. Safe.*, 2012, **79**, 288-293.

[6] K. E. Pelch, J. M. Beeman, B. A. Niebruegge, S. R. Winkeler and S. C. Nagel, *Hormones and Reproduction of Vertebrates.*, 2011, *Chapter 14*, 329-371.

[7] J. L. Tang-Peronard, H. R. Andersen, T. K. Jensen and B. L. Heitmann, *Obes. Rev.*, 2011, **12**, 622-636.

[8] G. R. Boyd, J. M. Palmeri, S. Zhang, and D. A. Grimm, *Sci. Total. Environ.*, 2004, **333**, 137-148.

[9] U.S. Environmental protection agency. (N.Y) *Pharmacuticals and Personal Care Products (PPCPs)*. Retrieved July 19, 2012, from http://www.epa.gov/ppcp/

[10] Environment Canada. (N.Y) *Pharmaceuticals and Personal Care Products in the Canadian Environment: Research and Policy Directions*. Retrieved July 19, 2012, from http://www.ec.gc.ca/inre-nwri/default.asp?lang=En&n=C00A589F-1&offset=9&toc=show

[11] M. J. Benotti, R. A. Trenholm, B. J. Vanderford, J. C. Holady, B. D. Stanford, and S. A. Snyder. *Environ. Sci. Technol.*, 2009, **43**, 597-603.

[12] K. McClellan, and R. U. Halden, *Water Research*, 2010, **44**, 658-668.

[13]   H. C. Zhang, X. J. Yu, W.C. Yang, J. F. Peng, T. Xu, D. Q. Yin and X. L. Hu, *J. Chromatogr B.*, 2011, **879**, 2998-3004.

[14]   T. C. G. Kibbey, L. Chen, N. Singhaputtangkul and D. A. Sabatini, *Chemosphere*, 2009, **76**, 1249-1257.

[15]   T.C.G. Kibbey, L. Chen, D. A. Sabatini, M. A. Mills, and C. Nietch, *Chemosphere*, 2010, **80**, 908-913.

[16]   J. C. C. Yu, A. Hrdina, C. Mancini and E. P. C. Lai, *J. Nanosci. Nanotechnol.*, 2007, **7**, 3095-3103.

[17]   S. Garg, C. Hurren and A. Kaynak, *Synth. Met.*, 2007, **157**, 41-47.

[18]   A. Schmid, L. R. Sutton, S. P. Armes, P. S. Bain and G. Manfrè, *Soft Matter.*, 2009, **5**, 407-412.

[19]   B. Lakard, L. Ploux, K. Anselme, F. Lallemand, S. Lakard, M. Nardin and J. Y. Hihn, *Bioelectrochemistry.*, 2009, **75**, 148-157.

[20]   L. Wang, J. Li, Q. Jiang and L. Zhao, *Dalton Trans.*, 2012, **41**, 4544-4551.

[21]   X. M. Li, G. Xu, Y. Liu and T. He, *Nanosci. Nanotechn. Asia.*, 2011, **1**, 14-24.

[22]   H. Parham, B. Zargar and R. Shiralipour. *J. Hazard. Mater.*, 2012, **205-206**, 94-100.

[23]   L. Han, and Y. Wei, *Mater. Lett.*, 2012, **70**, 1-3.

[24]   A. Afkhami and R. Moosavi, *J. Hazard. Mater.*, 2010, **174**, 398-403.

[25]   C. Wang, H. Zhang, Y. Chen, F. Shi and B. Chen, *Int. J. Nanomed.*, 2012, **7**, 781-787.

[26]   M. R. Shishehbore, A. Afkhami and H. Bagheri, *Colloids Surf. B.*, 2011, **82**, 316-324.

[27]   L. Chen, T. Wang and J. Tong, *Trends. Anal. Chem.*, 2011, **30**, 1095-1108.

[28]   T. Madrakian, A. Afkhami, M. A. Zolfigol, M. Ahmadi, and N. Koukabi, *Nano-Micro letters,.* 2012, **4**, 57-63.

[29]   J. Song, H. Kong, J. Jang, *J. Colloid Interf. Sci.*, 2011, **359**, 505-5011.

[30]   F. Ge, M.M. Li, H. Ye, and B. Zhao, *J. Hazard. Mater.*, 2012. **211-212**, 366-372.

[31]   D. Duranoglu, I. G. B. Kaya, U. Beker, and B. F. Senkal. *Chem. Eng. J.*, 2012,**181-182**, 103-112.

[32]   F. Ge, H. Ye, M.M. Li, and B.X. Zhao, *Chem. Eng. J.*, 2012.**198-199**, 11-17.

[33]   S. Shariati, M. Faraji, Y. Yamini, and A. A. Rajabi, *Desalination*, 2011, **270**, 160-165.

[34]   B. S. Inbaraj, and B.H. Chen, *Bioresource Technol.*, 2011, **1102**, 8868-8876.

[35]   X. Zhang, S. Xie, M. C. Paau, B. Zheng, H. Yuan, D. Xiao, and M.M.F. Choi, *J. Chromatogr. A.*, 2012. **1247**, 1-9.

[36]   L. P. Melo, A. M. Nogueira, F. M. Lancas, and M. E. C. Queiroz, *Anal. Chim. Acta.*, 2009, **633**, 57-64.

[37]   Yao, T.Cui, J.Wu, Q. Chen, S. Lu, and K. Sun, *Polym. Chem.*, 2011, **2**, 2893.

[38]   Afkhami, R. Moosavi and T. Madrakian, *Talanta.*, 2010, **82**, 785-789.

[39]   J. Meng, J. Bu, C. Deng and X. Zhang, *J. Chromatogr. A.*, 2011, **1218**, 1585-1591.

[40]   Y.Wan, D. Zhang, Y.Wang, P. Qi, and B. Hou, *Biosens. Bioelectronics*, 2011, **26**, 2595-2600.

[41]   J. Ou, J. Wang, J. Zhou, S. Liu,Y. Yu, X. Pang, and S. Yang, *Progr. Org. Coating.*,
       2010, **68**, 244-247.

[42]   B. D. McCloskey, H. B. Park, H. Ju, B. W. Rowe, D. J. Miller, B. J. Chun, K. Kin,
       and B.D. Freeman, *Polymer,* 2010, **51**, 3472-3485.

[43]   N. Farnard, K. Farhadi, and N. H. Voelcker. *Water Air Soil Pollut.*, 2012, DOI
       10.1007/s11270-012-1131-7.

[44]   M. Zhang, X. Zhang, X. He, L. Chen, and Y. Zhang. *Nanoscale*, 2012, **4**, 3141.

[45]   Z. Iqbal, E. P. C. Lai, and T. J. Avis, *Microchim Acta.*, 2011, DOI 10.1007/s00604-
       011-0712-2.

[46]   U. Pyell, *Electrophoresis*, 2010, **31**, 814-831.

[47]   S. P. Radko, and A. Chrambach, *Electrophoresis*, 2002, **23**, 1957-1972.

[48]   C. Quang, S. L. Peterson, G. R. Ducatte, N. E. Ballou, et al., *J. Chromatogr. A.*,
       1996, **732**, 377-384.

[49]   F. K. Liu, F. H. Ko, P. W. Huang, C.H. Wu, and T.C. Chu, *J. Chromatogr. A.*,
       2005, **1062**, 139-145.

[50]   F. K. Lui, Y. Y. Lin, and C. H. Wu, *Anal. Chim. Acta.*, 2005, **528**, 249-254.

[51]   V. G. Vanifatova, B.Y. Spivakov, and J. Mattusch, *Talanta,* 2005, **66**, 605-610.

[52]   H. K. Jones, and N. E. Ballou, *Anal. Chem.*, 1990, **62**, 2484-2490.

[53]   N. E. Baryla, and C. A. Lucy, *Anal. Chem.*, 2000, **72**, 2280-2284.

[54]   M.J. Schmerr, and A. Jenny, *Electrophoresis*, 1998, **19**, 409-414.

[55]   X. Song, L. Li, H. Qian, N. Fang, and J. Ren, *Electrophoresis*, 2006, **27**, 1341-
       1346.

[56] M. Pereira, and E.P.C. Lai, *J. Nanobiotechnology.*, 2008, *6*: 10. doi:10.1186/1477-3155-6-10.

[57] Z. Iqbal, S. Alsudir, M. Miah and E. P. C. Lai, *Electrophoresis*, 2011, **32**, 2181-2187.

[58] M. Clara, B. Strenn, E. Saracevic and N. Kreuzinger, *Chemosphere.*, 2004, **56**, 843–851.

[59] E. P. C. Lai and S. Y. Feng, *J. Chromatogr. B.*, 2006, **843**, 94–99.

[60] Y. Wang, W. Chen, D. Zhou and G. Xue, *Macromol. Chem. Phys.*, 2009, **210**, 936-941.

[61] C. Tixier, H. P. Singer, S. Canonica and S. R. Muller, *Environ. Sci. Technol.*, 2002, **36**, 34-3489.

[62] S. Strauch, J. B. Dressman, V. P.Shah, S. Kopp, J. E. Polli, and D. M. Brends. 2011. *Wiley Online library (wileyonlinelibrary.com)*. Doi 10.1002/jps.22810.

[63] R. Weinberger, *Practical capillary electrophoresis*, Academic Press Inc, San Diego, USA, 1993.

[64] Wikipedia (N.Y) *Capilllary electrophoresis*. Retrieved June 28, 2012 from http://en.wikipedia.org/wiki/Capillary_electrophoresis.

[65] BECKMAN COULTER (N. Y) *Electroosmotic Flow (EOF)*. Retrieved June 29, 2012 from https://www.beckmancoulter.com/wsrportal/wsr/research-and-discovery/products-and-services/capillary-electrophoresis/electroosmotic-flow/index.htm.

[66] M. J. Gordon, X. Huang, S. L. Pentoney, and R. N. Zara, *Science*, 1988, **242**, 224-228.

[67] D. C. Harris, *Quantitative Chemical Analysis*, Seventh Edition, W. H. Freeman and Company, New York 2006.

[68] B. S. Inbaraj, and B. H. Chem, *Bioresorce Technol.*, 2011, **102**, 8868-8876.

[69] R. Ansari, and A. Pornahad, *Sep. Sci. Technol.*, 2010. **45**, 2376-23823.

[70] G. Wang, W. Tang, X. Hao, C. Yan, and Y. Lu,. *J. Biophys. Chem.*, 2011. **2**, 194-201.

[71] F. Lu, H. Li, M. Sun, L. Fan, H. Qiu, X. Li, and C. Luo, *Anal. Chim. Acta.*, 2012. **718**, 84-91.

[72] M. Macka, P. Andersson, P. Haddad, *Anal. Chem.*, 1998, **70**, 743-749.

[73] X. Wang, L. Wang, X. He, Y. Zhang and L. Chen, *Talanta*, 2009, **78**, 327-332.

[74] H. Z. Wen, H. L. Chun, C. G. Xiu, R. C. Fa, H. Y. Huang, and R. W. Xiao, *J. Mater. Chem.*, 2010, **20**, 880-883

[75] Z. Min, Z. Xihao, H. Xiwen, C. Langxing, and Z. Yukui, *Nanoscale*, 2012. **4**, 3141-3147.

[76] G. Qui, Q. Wang, and M. Nie, *Macromol. Mater. Eng.*, 2006, **291**, 68-74.

[77] T. Yao, T. Cui, J. Wu, Q. Chen, S. Lu, and K. Sun, *Polymer chemistry*, 2011, **2**, 2893.

[78] M. J. Antony and M. Jayakannan, *J. Phys. Chem. B.*, 2007, **111**, 12772-12780.

[79] L. P. Zhu, J. H. Jiang, B. K. Zhu, and Y.Y. Xu, *Colloid. Surface. B.*, 2011, **86**, 111-118.

[80] J. Jang, and H. Yoon, *Adv. Mater.*, 2003, *15*, 2088-2091.

[81] A. Hrdina, E.P.C. Lai, C.S. Li, B. Sadi and G. Kramer, *J. Magn. Magn. Mater.*, 2010, **322**, 2622-2627.

[82] T. Yao, T. Cui, J. Wu, Q. Chen, S. Lu, and K. Sun, *Polymer chemistry*, 2011, **2**, 2893.

[83] Y. C. Liu, B. J. Hwang, *Thin Solid Films*, 2000, **360**, 1.

[84] Y.Ren, J.G. Rivera, L. He, H. Kulkarni, D.K. Lee, and P.B. Messersmith, *BMC Biotechnology*, 2011, **11**, 63.

[85] E. Duguet, S. Vasseur, S. Mornet, J.M. Devoisselle, *Nanomedicine*, 2006, **1**, 157-168.

[86] L. Wang, J. Li, Q.Jiang, and L.Zhao, *Dalton Transactions*, 2012, **41**, 4544

[87] W.Wang, Y. Jiang, Y. Liao, M. Tian, H. Zou, and L. Zhang, *J. Colloid. Interf. Sci.*, 2011, **358**, 567-574.

[88] N. Farnard, K. Farhadi, and N. H. Voelcker, *Water Air Soil Pollut.*, 2011, DOI 10.1007/s11270-012-1131-7.

[89] M. Omastova, and M. Micusik, *Chem. Pap.*, 2012, **66**, 392-414.

[90] A. G. Badgujar, V.A. Bambole, and P. A. Mahanwar, *Paintindia*, 2011, **61**, 53-66.

[91] R. Ansari, M. B. Keivani, and A.F. Delavar, *J. Appl. Polym. Sci.*, 2011, **122**, 804-812.

[92] P. Olszowy, M. Szultka, T. Ligor, J. Nowaczyk, and B. Buszewski, *J. Chromatogr.*, 2010, **878**, 2226-2234.

[93] L.P. Melo, A.M. Nogueira, F.M. Lancas, and M.E. Queiroz, *Anal. Chim. Acta.*, 2009, **633**, 57-64.

[94] J.C.C. Yu, E.P.C. Lai, *Anal.Bioanal. Chem.*, 2005, **381**, 948-952.

[95] Q. Gao, D. Luo, M. Bai, Z.W. Chen, and Y.Q. Feng, J. Agric. Food Chem., 2011, **59**, 8543-8549.

[96]   C. Raji, and T. S. Anirudhan, *Indian J. Chem.Techn.*, 1997, **4**, 228-236.

[97]   M. Bhaumik, A. Maity, V.V. Srinivasu, and M.S. Onyango, *J. Hazard.Mater.*, 2011.**190**. Page: 381-390.

[98]   J. Pan, H. Yao, X. Li, B. Wang, P. Huo, W. Xu, H. Ou, and Y. Yan,. *J. Hazard.Mater.*, 2011.**190**, 276-284.

[99]   F. Ge, H. Ye, M.M. Li, and B.X. Zhao, *Chem. Eng. J.*, 2012.**198-199**, 11-17.

[100]   C. Chen, X. Jiang, Y.V. Kaneti, and A. Yu, *Powder Technol.*, In Press, Corrected Proof, Mar 2012.

[101]   S. K. Sahu, S. Maiti, A. Pramanik, S. K. Ghosh, and P. Pramanik, *Carbohydr. Polym.*, 2012. **87**, 2593-2604.

[102]   B. H. Lai, C.C. Yeh, and D.H. Chen, *Process Biochem.*, 2012. **47**, 799-805.

[103]   I. Perçin, V. Karakoç, S. Akgöl, E. Aksöz, and A. Denizli, *Mater. Sci. Eng., C*, 2012. **32**, 1133-1140.

[104]   A. Akbarzadeh, H. Mikaeili, N. Zarghami, R. Mohammad, A. Barkhordari and S. Davaran, *Int. J. Nanomed.*, 2012, **7**, 511-526.

[105]   S.Y. Liu, Y.Han, L.P. Yin, L.Long, and R. Liu, *Adv. Mater. Res.*, 2008, **47**, 1097-1100.

[106]   A.K. Gupta, and S. Wells, *IEEE Trans Nanobioscience*, 2004, **3**, 66-73.

[107]   Wahajuddin and S. Arora, *Int. J. Nanomed.*, 2012, **7**, 3445-3471.

[108]   A.K. Gupta, M. Gupta, *Biomaterials*, 2005, **26**, 1565-1573.

[109]   A. Petri-Fink, M. Chastellain, L. Juillerat-Jeanneret, A. Ferrari, and H. Holfmann, *Biomaterials*, 2005, **26**, 2685-2694.

[110]   X. Wang, X. Gu, C. Yuan, S. Chen, P. Zhang, T. Zhang, J. Yao, F. Chen, and G.

Chen, *J. Biomed. Mater. Res.*, 2004, **68A**, 411-422.

[111]   Wikipedia (N.Y) *Capilllary electrophoresis*. Retrieved July 28, 2012 from

http://en.wikipedia.org.